

Tesis defendida por

Florian Neumann

y aprobada por el siguiente Comité

---

Dr. Juan Contreras Pérez

*Director del Comité*

---

Dr. Edgardo Cañón Tapia

*Miembro del Comité*

---

Dr. Alejandro Parés Sierra

*Miembro del Comité*

---

Dr. Gustavo Tolson Jones

*Miembro del Comité*

---

Dr. Antonio González Fernández

*Coordinador del programa de  
posgrado en Ciencias de la Tierra*

---

Dr. David Hilario Covarrubias Rosales

*Director de Estudios de Posgrado*

10 de diciembre de 2012

CENTRO DE INVESTIGACIÓN CIENTÍFICA Y DE  
EDUCACIÓN SUPERIOR DE ENSENADA



---

Programa de Posgrado en Ciencias  
en Ciencias de la Tierra

---

An analog model of the Middle American subduction zone  
and the mantle flow beneath the Jalisco and Michoacan blocks

Tesis

que para cubrir parcialmente los requisitos necesarios para obtener el grado de

Maestro en Ciencias

Presenta:

Florian Neumann

Ensenada, Baja California, México

2012

Abstract of the thesis presented by Florian Neumann, in partial fulfillment of the requirements of the degree of Master in Sciences in Earth Science with orientation in Geology. Ensenada, Baja California, December 2012.

**An analog model of the Middle American subduction zone  
and the mantle flow beneath the Jalisco and Michoacan blocks**

Abstract approved by:

---

Dr. Juan Contreras Pérez

Director of Thesis

Laboratory modeling of the present-day Northern Middle American subduction zone is carried out to understand the mantle flow patterns beneath the Jalisco and Michoacan blocks. The scaled model consists of two polyethylene strips, which are forced into a tank filled with corn syrup at different angles and velocities. One of the strips dips  $60^\circ$  and moves at a velocity of 25 mm/min simulating the Rivera plate. The other one dips  $45^\circ$ , moves at 75 mm/min and represents the Cocos plate. One cm in the model represents 40 km in the natural scale whereas one minute represents eight million years. The syrup contains bead-like pasta to track down flow paths within the simulated mantle. The modeling brings to light how plate motions and their slab geometries control the mantle flow in the Northern Middle American subduction zone. The model shows the following. (1) Pasta beads at shallow depths in the modeled mantle wedge move toward the fast moving strip representing the Cocos plate. (2) The pasta beads situated close to the strips are carried down to the lower part of the tank. (3) Pasta beads situated in the simulated asthenospheric mantle, near the gap between the strips, first show a downgoing movement as they move through the gap, then they change direction and ascend into the modeled mantle wedge. These results reveal complex patterns of toroidal and corner flows. Model results are in agreement with seismic anisotropy studies and geochemistry of lavas erupted in the Jalisco and Michoacan blocks.

Keywords: **subduction zone, TMVB, mantle flow**

Resumen de la tesis de Florian Neumann, presentada como requisito parcial para la obtención del grado de Maestro en Ciencias en Ciencias de la Tierra con orientación en Geología. Ensenada, Baja California, Diciembre de 2012.

### **Modelado analógico de la zona de subducción de Mesoamérica y el flujo del manto abajo de los bloques de Jalisco y Michoacán**

Para entender los patrones de flujo del manto por debajo de los bloques de Jalisco y Michoacán, se llevó a cabo modelado analógico de la parte norte de la zona de subducción de mesoamérica. El modelo escalado consta de dos tiras de polietileno las cuales son forzadas en un tanque con jarabe de maíz a diferentes ángulos y velocidades. Una de las tiras entra en el jarabe con un ángulo de  $60^\circ$  y se mueve a una velocidad de 25 mm/min simulando la placa de Rivera. La otra tiene un ángulo de  $45^\circ$ , se mueve a 75 mm/min y representa la placa de Cocos. Un cm en el modelo representa 40 km a escala natural, mientras que un minuto equivale a ocho millones de años. El jarabe contiene lentejas de pasta como trazadores de las trayectorias de flujo del manto simulado. El modelo pone de manifiesto cómo los movimientos de las placas y las geometrías de las losas controlan el flujo en el manto en la zona de subducción del norte de Mesoamérica. El modelo muestra lo siguiente. (1) Pasta a poca profundidad en la cuña del manto modelado se mueve hacia la tira de movimiento rápido que representa la placa de Cocos. (2) La pasta situada cerca de las tiras descienden hacia la parte inferior del tanque. (3) La pasta situada en el manto astenosférico simulado, cerca de la brecha entre las bandas, primero muestran un movimiento descendente mientras se mueven a través de la brecha, y luego cambian de dirección y ascienden hacia la cuña del manto modelado. Estos resultados revelan patrones complejos de flujos toroidales y poloidales (flujo de esquina). Los resultados del modelo están de acuerdo con estudios de anisotropía sísmica y geoquímica de las lavas eruptadas en los bloques de Jalisco y Michoacán.

Palabras Clave: **zona de subducción, FVTM, flujo en el manto**

*Für den gläubigen  
Menschen steht Gott  
am Anfang, für den  
Wissenschaftler am  
Ende aller seiner  
Überlegungen*

*Max Planck*

# Acknowledgement

Quiero agradecer al CICESE por el apoyo y por usar las instalaciones. Al CONA-CyT y proyecto de investigación por su apoyo económico.

Un gran agradecimiento quiero dar a mi director de tesis Dr. Juan Contreras, por su comprensión, apoyo, paciencia, conocimiento y sinceridad durante mis dos años. Para mí fueron dos años especiales con buenas discusiones y pláticas con Juan. Muchas gracias.

A mis sinodales por los comentarios durante los avances y por su puerta abierta cuando tenía preguntas o dudas. En especial al Dr. Edgardo Cañón, al Dr. Alejandro Parés y al Dr. Gustavo Tolson. Gracias por su tiempo.

Le agradezco a la UNAM por permitirme trabajar y realizar mis experimentos en el laboratorio de modelos analógicos, en especial a Gustavo Tolson por sus ideas, comentarios y su apoyo económico. Además quiero agradecer a Beto por su ayuda en los cambios del experimento y en la realización de ellos, al Ing. Teodoro Hernández por permitirme trabajar en su taller y su ayuda en la construcción del modelo analógico.

Agradezco a mis maestros durante estos dos años, a los técnicos y al personal administrativo. Un agradecimiento especial para Martha Barrera, que siempre se encarga de todo y de todos los estudiantes para que salgan las cosas bien. A Mari Carmen, Enid Morán, Magdalena Chávez, José Mojarro, Sergio Arregui, Humberto Benitez, Pratap Sahay y al Antonio González. Además a servicios escolares en especial a Ivonne Best

por la ayuda de tramitar la beca, a Norma Fuentes y Dolores Sarracino por su paciencia y el apoyo durante el proceso de ingreso. Al Dr. Rogelio Vázquez por su apoyo durante un verano en el cual conocí el CICESE y decidí realizar la maestría.

A mis compañeros del CICESE, el equipo del hockey, los Halcones y amigos por su compañía, las buenas pláticas y convivios. Gracias especialmente para: Nancy, Samuel, Mine, Cristina, Javier, Clemente, Ale, Viri, Tomas, Gina, Claudia, Nestor, Angelica, Gemma, Roman, Armando, Mario, Porfirio, Orlando, Ekaterina, las vecinas, Faride, Joao, Ivan, Adrian, Veronica y a todos que se me olvidaron.

Mein ganz besonderer Dank gilt abschliessend meiner Mutter und meiner Schwester, die mich immer unterstützt haben und mir stets helfend zur Seite standen. Des Weiteren meiner Freundin Xochitl für viele anregende Diskussionen, fortwährende Motivation und einen liebevollen Beistand während der gesamten Arbeit und meinen langjährigen Freunden Timm, Hanna, Steffi, Mario und Kathrin.

# Contents

<b>Abstract in English</b>	<b>i</b>
<b>Abstract in Spanish</b>	<b>ii</b>
<b>Dedication</b>	<b>iii</b>
<b>Acknowledgement</b>	<b>iv</b>
<b>List of Figures</b>	<b>vii</b>
<b>List of Tables</b>	<b>viii</b>
<b>I. Introduction</b>	<b>1</b>
<b>II. Experimental set-up</b>	<b>9</b>
II.1 Similarity and nondimensional analysis . . . . .	14
II.2 Model limits . . . . .	18
<b>III. Results</b>	<b>20</b>
<b>IV. Discussion</b>	<b>33</b>
<b>Conclusions</b>	<b>37</b>
<b>References</b>	<b>38</b>

# List of Figures

Figure		Page
1	Overview map of the study area . . . . .	2
2	General subduction geometry of Rivera and Cocos plate . . . . .	3
3	P wave velocity model beneath Jalisco and Michoacan block . . . . .	4
4	SKS and SKKS shear wave splitting measurements of southern Mexico .	6
5	Subduction tank with equipment . . . . .	10
6	Polyethylene strips . . . . .	12
7	Cleaning station . . . . .	13
8	Pasta beads . . . . .	13
9	Top view of the flow patterns in the mantle wedge . . . . .	21
10	Top view of the flow patterns in the mantle wedge . . . . .	22
11	Location for the mantle wedge experiments . . . . .	23
12	Location for the asthenospheric mantle experiments . . . . .	24
13	Flow patterns in the mantle wedge above the Rivera plate . . . . .	25
14	Flow patterns in the mantle wedge above the gap . . . . .	26
15	Flow patterns in the mantle wedge above the Cocos plate . . . . .	27
16	Flow patterns in the asthenospheric mantle above the Rivera plate . . . .	29
17	Flow patterns in the asthenospheric mantle above the gap . . . . .	30
18	Flow patterns in the asthenospheric mantle above the Cocos plate . . . .	31
19	Merged results . . . . .	32

# List of Tables

Table		Page
I	Summary of the features in the study area . . . . .	1
II	Units and parameters for mantle convection . . . . .	15
III	Scaling parameters in nature and the laboratory model . . . . .	18
IV	Experimental set ups . . . . .	20

# Chapter I

## Introduction

The northern part of the Middle American Subduction Zone (MASZ) has an unique configuration on Earth where a mayor tectonic plate is being fragmented into a series of smaller plates (Stock & Lee, 1994, Fig. 1). Plate reconstructions shows that about 23 Ma ago the Cocos plate fragmented from the Farallon plate (Lonsdale, 2005; Mann, 2007). 13 Ma later, the Rivera plate, the smallest remaining fragment of the Farallon plate separated from the Cocos plate (DeMets & Traylen, 2000). Presently, those two oceanic plates are being subducted at different angles and rates underneath the North America plate creating a volcanic arc, the Trans-Mexican Volcanic Belt (TMVB).

On one hand, seismic tomography (Yang *et al.*, 2009) shows that the Rivera plate

Table I: Summary of the features in the study area. Modified from Ferrari *et al.* (2012) and Yang *et al.* (2009)

Sector	Western (Jalisco)	Central (Michoacan)
Geographic Boundaries	West of 103°00'W	103°00'W-100°30'W
Subducting plate	Rivera	Cocos west of Orozco FZ
Plate age at trench	~10 Ma	11-17.6 Ma
Slab dip	60°	45°
Subduction rate	~2 cm/yr	~6 cm/yr
Crust thickness beneath the arc	35 to 40 km	35 to 40 km
Silicic volcanism	Abundant, mostly large domes complexes, less ignimbrites. Only emplaced in the rear half of the arc	Almost absent
Intraplate alkaline (OIB) volcanism	Since Early Pliocene in the rear part of the arc	Rare in the Pleistocene at the arc front (Michoacan-Guanajuato volcanic field)

dips  $60^\circ$  beneath the TMVB (DeMets & Traylen, 2000). Moreover, analysis of magnetic anomalies indicate this plate is being subducted at a rate of 2 cm/yr. The Cocos plate, on the other hand, dips  $45^\circ$  under the TMVB and moves at a rate of 3.8 cm/yr, increasing rapidly southwards to values up to 6.4 cm/yr along the Acapulco subduction zone (Fig. 1). On the basis of seismicity, earthquake tensor solutions and slab geometries the deformation on the upper plate caused by the MASZ became localized along the

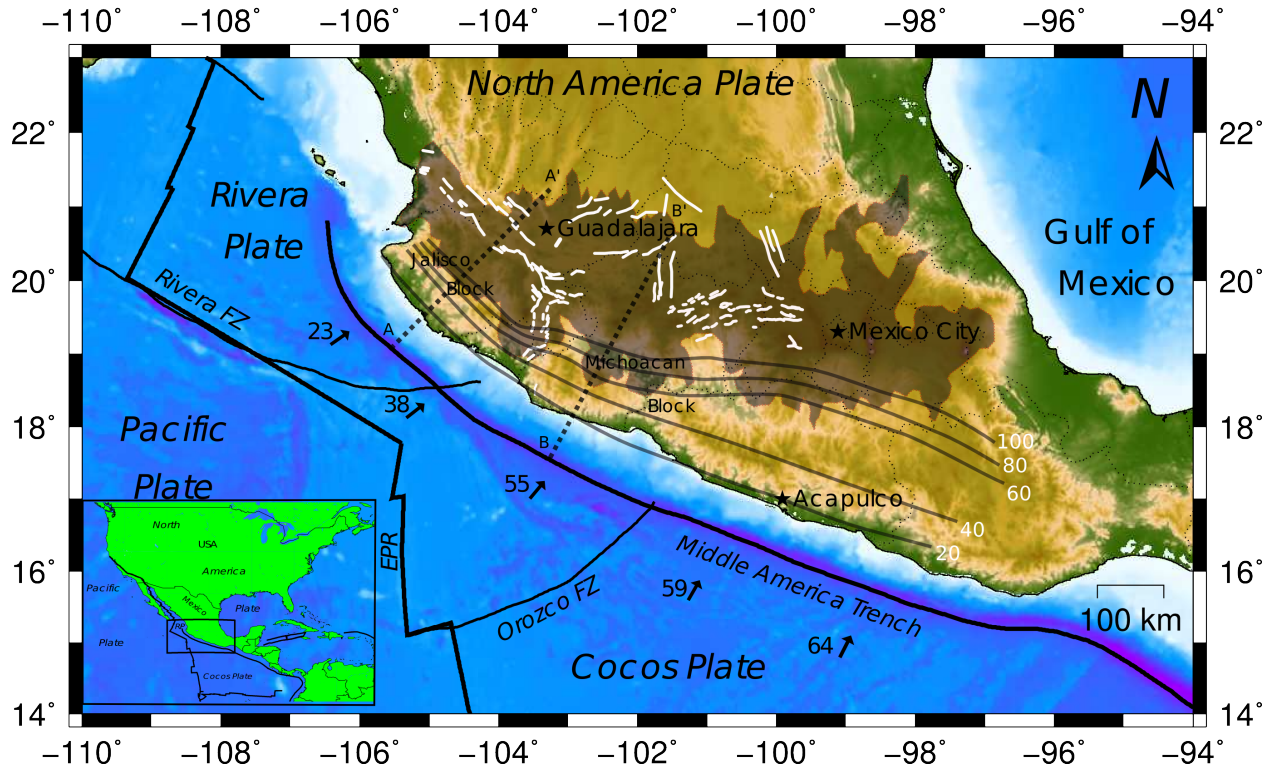


Figure 1: Map outlining the TMVB (shaded zone), the main plate tectonic features and mayor fault zones in south western Mexico. Contours indicate the depth in km of the Wadati-Benioff zone (Pardo & Suarez, 1995). Arrows show direction and relative convergence rate in mm/yr at the trench (Ferrari *et al.*, 2012). Dashed lines correspond to the location of profiles in Figure 2 . FZ = Fracture zone; EPR = East pacific Rise; RP = Rivera plate.

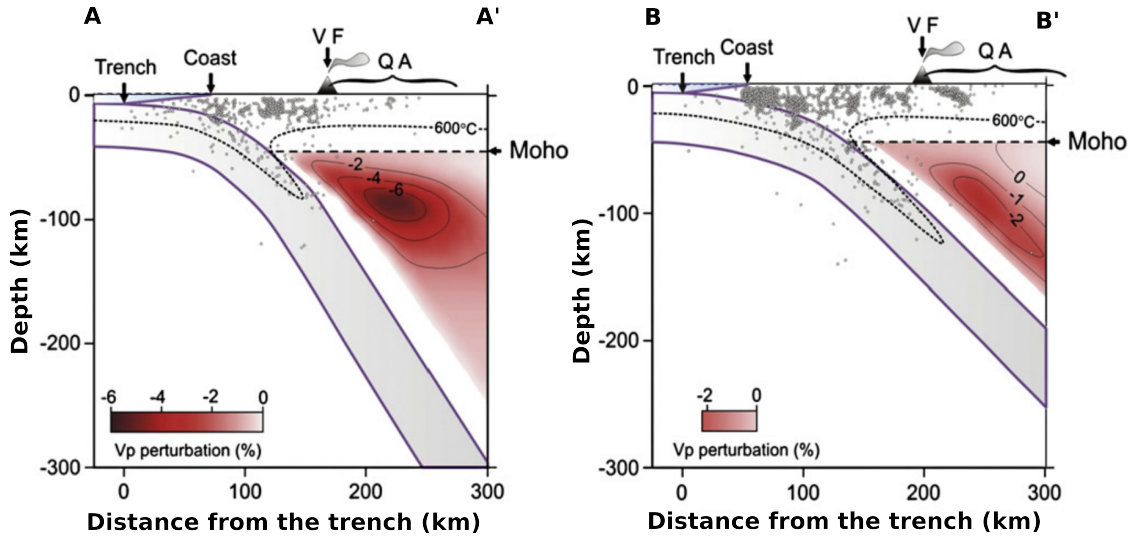


Figure 2: Mantle wedge models for the Rivera - North America and Cocos - North America subduction zone for the profiles in Figure 1 (Ferrari *et al.*, 2012). Dots represent seismic events. Colors show the synthetic  $V_p$  perturbation from bright red (0%) to a negative velocity anomaly (max -6%). VF = Volcanic Front; QA = Quaternary Arc;

boundaries of the Jalisco and Michoacan blocks and along the axis of the TMVB (Pardo & Suarez, 1995, Fig. 1). A detailed summary of the Jalisco and Michoacan blocks is presented in Table I and a schematic view of the general subduction geometry of the northern MASZ is shown in Figure 2.

Another feature of the northern MASZ is a gap between the two plates at a depth of 200 km (Yang *et al.*, 2009, Fig. 3). The gap was imaged by seismic tomography of seismic events recorded during the MARS (Mapping the Rivera Subduction Zone) and CODEX (Colima Volcano Deep Seismic Experiment) experiments (Yang *et al.*, 2009; Gardine *et al.*, 2007). The tomography shows a high velocity band parallel to the trench, which follows the slab contours of the Rivera and Cocos plates. Furthermore, notice that with increasing depth the amplitude of the velocity anomaly decreases and that the Cocos plate is visibly farther from the trench indicating a shallower subduction angle with respect to the Rivera plate. The strike of the Rivera plate as seen from 200 km to 380 km depth slices in Figure 3 is east-west. The gap is seen as an interruption

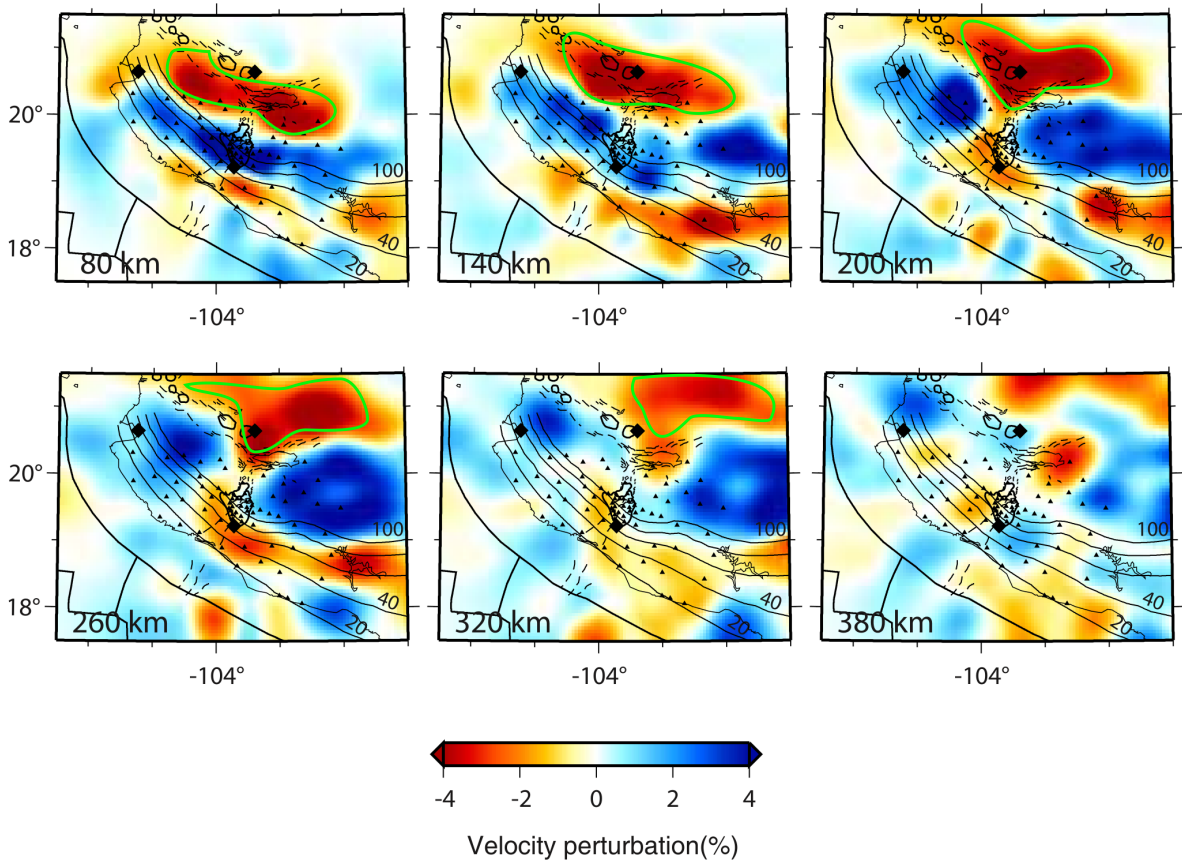


Figure 3: P wave velocity model beneath the Jalisco and Michoacan blocks (Yang *et al.*, 2009). Slab contours, seismic stations and geological settings are shown in each horizontal slice. The green contour marks a low velocity region.

of the high velocity band at a depth  $\sim 200$  km to  $\sim 320$  km. The gap vanishes at depths greater than 380 km. The gap marks the plate boundary between the Rivera and Cocos plates and its surface location is west of the Colima Rift. The tomography also reveals the presence of low velocity mantle under the western section of the TMVB and the Los Altos de Jalisco area (Fig. 3). This low velocity band loses expression at a depth of  $\sim 380$  km. Note, however, that a connection exists between the band and the gap at a depth of 200 km. Furthermore a recent study Perez-Ramirez *et al.* (2012) affirms the results from Yang *et al.* (2009) but indicates the gap is located at a shallower depth around 60 km.

A further complexity related to the unique setting of the northern MASZ is the presence of high temperature magmas of oceanic-island basalt (OIB) affinity (Ferrari *et al.*, 2001; Gómez-Tuena *et al.*, 2007; Vigouroux *et al.*, 2008). Clearly, such geochemical composition is not related to the metasomatized mantellic sources of subduction zones, as they have their origin in the deep undepleted mantle. What is more, controversially the OIB volcanism is often observed in close association with rifting of continental lithosphere and mantle upwelling elsewhere. These observations have led to some authors to propose that western Mexico is in the processes of breaking up (Luhr *et al.*, 1985; Allan, 1986; Marquez *et al.*, 1999; Verma, 2002, 2009), although this hypothesis is dubious (Contreras, 2012). Regardless of their origin, the presence of OIB magmas in the volcanic arc are indicative of mixing in the mantle wedge of the northern MASZ. An idea that has gained popularity recently is that mixing is a product of toroidal flow through the gap and around the northwestern edge of the Rivera plate and advection of asthenospheric material by corner flow induced by subduction. These phenomena are the result of slab rollback of the Rivera plate (Ferrari, 2004; Yang *et al.*, 2009; Ferrari *et al.*, 2012).

Seismic anisotropy studies by Soto *et al.* (2009) lend support to this idea (Fig. 4). Seismic anisotropy in the upper mantle is the product of the elongated olivine crystals, which tend to align parallel to the mantle flow direction. In the crust, by contrast, anisotropy is caused by aligned joints or microfractures, layered bedding of sediments or foliation of metamorphic rocks. Anisotropy is estimated in the following way. Shear waves passing through an anisotropic media naturally split into separated arrivals with two polarizations directions. If the delay of the fast and slow arrivals is measured then the anisotropy can be established with some degree of accuracy. The larger the delay the smaller the uncertainty of the determination. Anisotropy measurements for southern Mexico are presented in Figure 4.

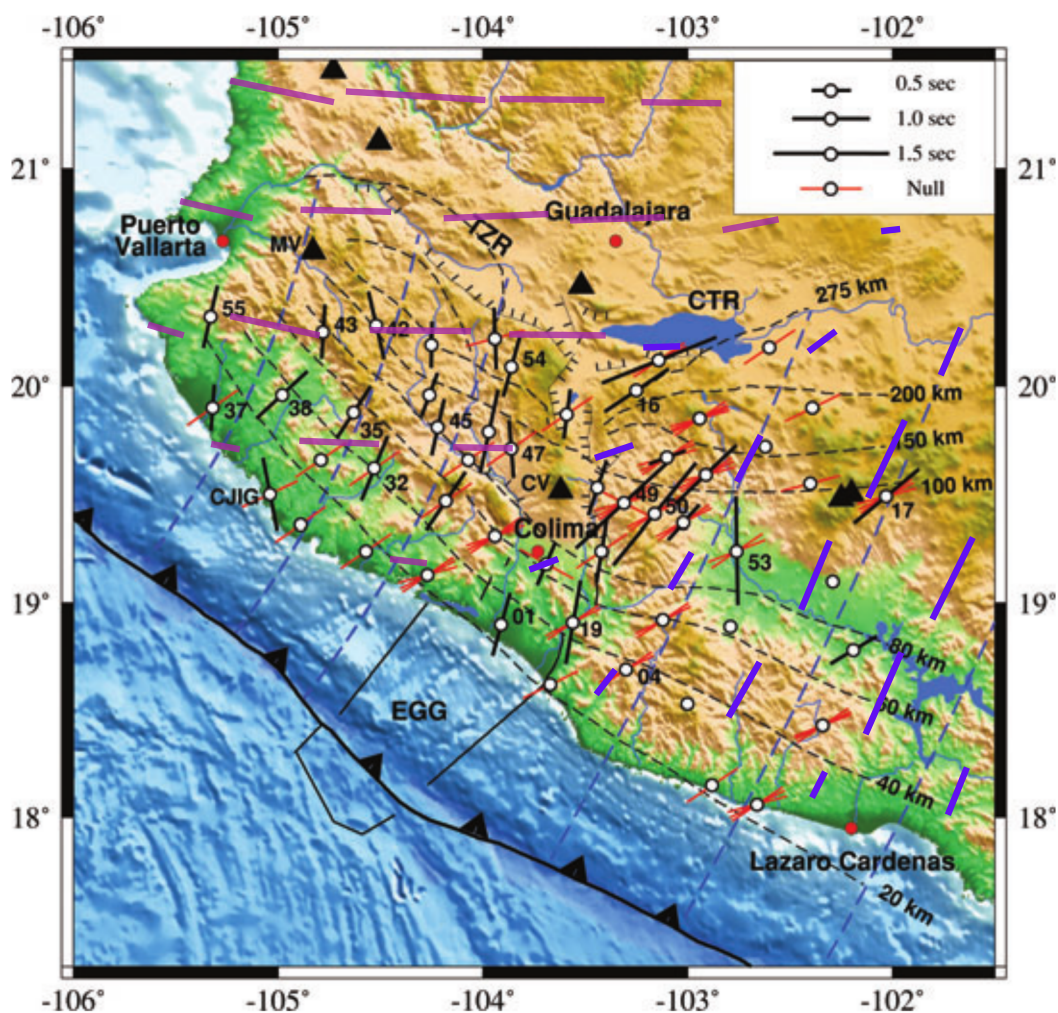


Figure 4: SKS and SKKS shear wave splitting obtained from the MARS experiment, modified from (Soto *et al.*, 2009; Stubailo *et al.*, 2012). Black bars show weighted average fast polarized direction with length proportional to their time delay. Red bars represents null measurements. Blue bars indicates confidential data within the well resolved area whereas purple bars are outside. Triangles show the recent volcanoes and dotted lines are contours of the Benioff zone (Pardo & Suarez, 1995; Yang *et al.*, 2009). TZR=Tepic Zocalco Rift; CTR=Chapala Tula Rift; EGG=El Gordo Graben; CV=Colima Volcano; MV= Mascota Volcano; CJIG= Station of Mexico's Servicio Sismológico Nacional

Black solid bars in that figure indicate fast direction of polarization; magnitude of bars are proportional to the time delay. It can be appreciated that maximum values of anisotropy tend to concentrate near the intersection of the Chapala and Colima graben.

Both west and east of the Colima Rift show similar anisotropy patterns to those of Soto *et al.* (2009). However, for the Cocos plate data density decreases towards the east. Red bars in the figure show null measurements with time delays less than 0.05 s and are mainly distributed east of the Colima Rift. Additionally blue and purple solid bars are measurements obtained by Stubailo *et al.* (2012), which show similar patterns. Purple bars are measurements with large uncertainties whereas blue ones are well resolved.

Anisotropy measurements in southern Mexico show that mantle flow diverges underneath the Jalisco and Michoacan blocks. The mantle under the Jalisco block has an anisotropy oriented NNE to due N, whereas under the Michoacan block is oriented NW. Furthermore, Soto *et al.* (2009) estimated that up to 0.8 s of the 1.0 s average time delay originates from anisotropy in the slab and subslab mantle (for measurements away from the trench) and from the slab, and underlying mantle (for measurements beneath the forearc).

Here, I present the results of an analog experiment for the northern section of the MASZ. The model uses materials that approximate reasonably well the rheology of the mantle and boundary conditions are consistent with geological and geophysical observations. The analog model consists a tank where corn syrup is placed on forced convection. The syrup has a viscosity of  $\sim 6.5$  Pa s and a density of  $1353$  kg/m<sup>3</sup>. The following boundary conditions are used for the analog model. The Rivera and Cocos plates are simulated by two polyethylene strips that move at a rate of 25 mm/min and 75 mm/min respectively. Above the fluid floats an acrylic plate that simulates the continental crust. Bead-like pasta was used to track down the different flowpaths within the simulated mantle.

Among the questions that will be touched on here are the following: Is it possible that, only from the convergence rate difference between the Cocos and Rivera plates, material enters through the gap into the mantle wedge? How is the flow pattern within the mantle wedge and what effect it has on mantle mixing? Does rollback play any role on the process? What is the origin of the low velocity anomaly north of the TMVB?

## Chapter II

### Experimental set-up

Here, I adopt the results obtained by tomography (Yang *et al.*, 2009), anisotropy (Soto *et al.*, 2009) and petrology studies (Ferrari *et al.*, 2001) that indicate a gap between the Rivera and Cocos plates exists under the Jalisco and Michoacan blocks. Based on these evidences I constructed an analog model of the northern MASZ. The idea behind analog models is to reproduce the mechanics of large scale problems in a scale that is manageable in a laboratory setting. This is specially true in Earth Sciences as the scale of terrestrial processes are in the order of hundreds of kilometers. The analog model used for this thesis consists of an acrylic tank in which a viscous fluid is set in forced convection. The subduction tank is show in Figure 5. Above the fluid floats a 0.2 cm thick acrylic plate, which represents the continental crust. The dimensions of the tank are the following: the tank is 1 m-long, 25 cm-wide and 75 cm deep. As discussed later on these dimensions permit experiments on a scale of 1:40,000,000 (1 cm in the model represents 40 km in nature).

Two polyethylene strips driven by a roller connected to a motor simulate the subducted slabs of the Rivera and Cocos plates beneath the North American plate. The analog model is best suited for the slab geometry proposed by Perez-Ramirez *et al.* (2012) in which the gap between the two plates is located at a shallow depth of 60 km. In the analog experiment, the Rivera plate dips at an angle of 60°; the Cocos does it at 45° (Fig. 6, Table I). The roller is comprised of two different diameters, which allows to simulate the different convergence rate of the Rivera and Cocos plates. One half of

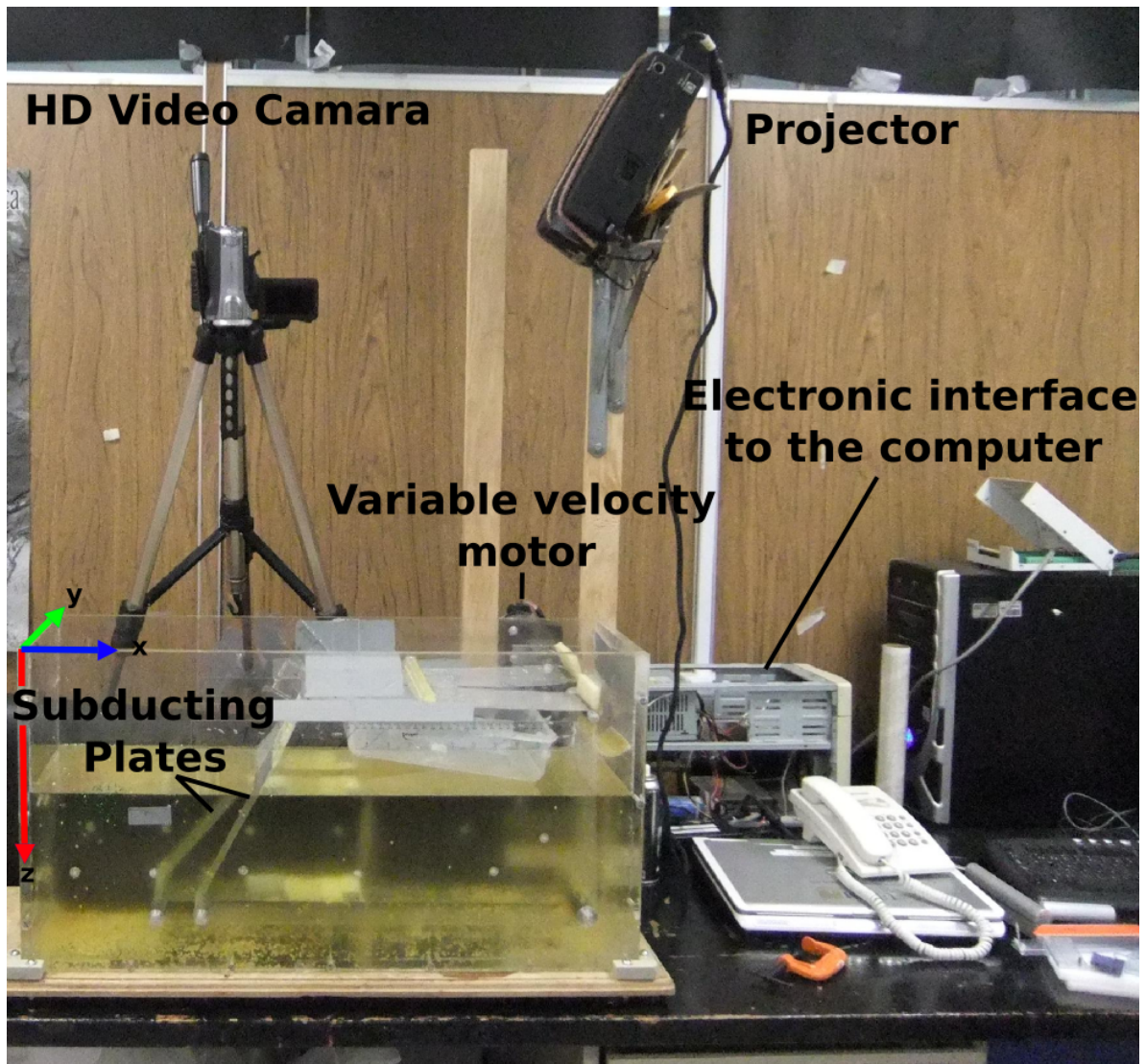


Figure 5: Experimental configuration of the subduction zone

the roller measures  $\varnothing$  1 cm whereas the other half is  $\varnothing$  3 cm. The roller was fabricated from a handlebar grip made of soft plastic. Sandpaper was glued to the roller to avoid friction slipping of the polyethylene strips. The motor is connected via an electronic interface to a computer controlling the velocity of the experiment.

The substance used to simulated the mantle is corn syrup (Heuret *et al.*, 2007). Several are the reasons to use this material: (i) is easy to handle in the laboratory and

to obtain in large batches, (ii) is cheap and, (iii) is biodegradable. Furthermore, the properties of corn syrup do not change significantly between one corncob and another. Another important property is that it flows in a Newtonian fashion, i.e., stress is a linear function of strain rate. This is relevant because non-Newtonian fluids are difficult to handle and characterize. During the experiment Karo-brand corn syrup was used. I estimated the viscosity of the corn syrup at 6.4 Pa·s using the Stokes experiment. The construction of the tank, which allows adjusting the angle and tension of polyethylene strips (Fig. 6), includes two sliding acrylic support bars in the upper part and two horizontally-separated aluminum rollers in the bottom part of the tank forming a conveyor belt. Additionally, a cleaning station was engineered to get rid of syrup attached to the strips once they come out of the syrup. The strips pass between two acrylic bars covered with styrofoam soaked in water. To keep the properties of the syrup constant, a recipient was installed below the foam-covered sticks (see Fig. 7) to avoid any mixing with the water used for cleaning the strips.

The velocity of the motor was set to a fixed value of 50 mm/min for the duration of all the experiments. At this velocity, experiments have a reasonably low Reynolds number (see discussion below). At the same time, it keeps the running time of the experiments practical. On average experiments lasted  $\sim 10$  min.

To analyze the flow patterns emerging from the analog simulation, pasta beads of anchellini were embedded in the syrup (Fig. 8). The pasta was inked for better contrast during the recording of the experiment's results. It is important to notice that uncooked anchellini is slightly negatively buoyant (sinks) in corn syrup whereas boiled is positive buoyant (floats). The former behavior allowed to record flow patterns at different depths by giving time for the pasta beads to settle ahead of starting the experiments.

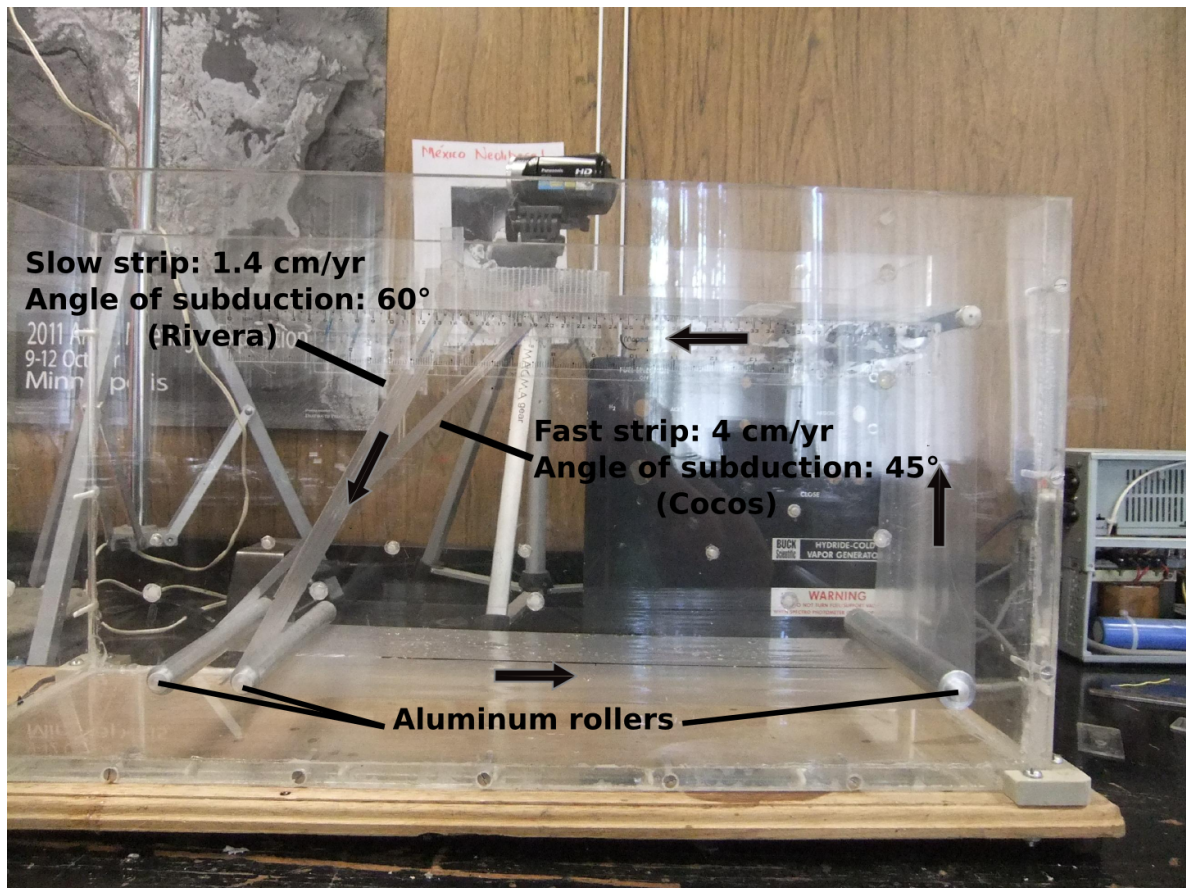


Figure 6: Lateral view with the two polyethylene strips representing the Rivera and Cocos plate with convergence rate (cm/yr)

Experiment results are recorded by two digital cameras. One mounted above the tank recording flow in the “xy” plane of the tank (video HD). Another one is placed on the side recording flow in the “xz” plane (digital camera 5 Mp). Images from the recorded videos were extracted every 10 to 20 seconds, depending on the length of the recordings. Then, the motion of individual particle markers were tracked down using two different approaches. For the first one, I used an automatic detection of particles JAVA-based plug-in of the image processing program ImageJ (ImageJ (2004)). The plug-in was developed by the MOSAIC (MOdels, Simulations, and Algorithms for Interdisciplinary Computing (MOSAIC (2009)) group and its mathematical foun-

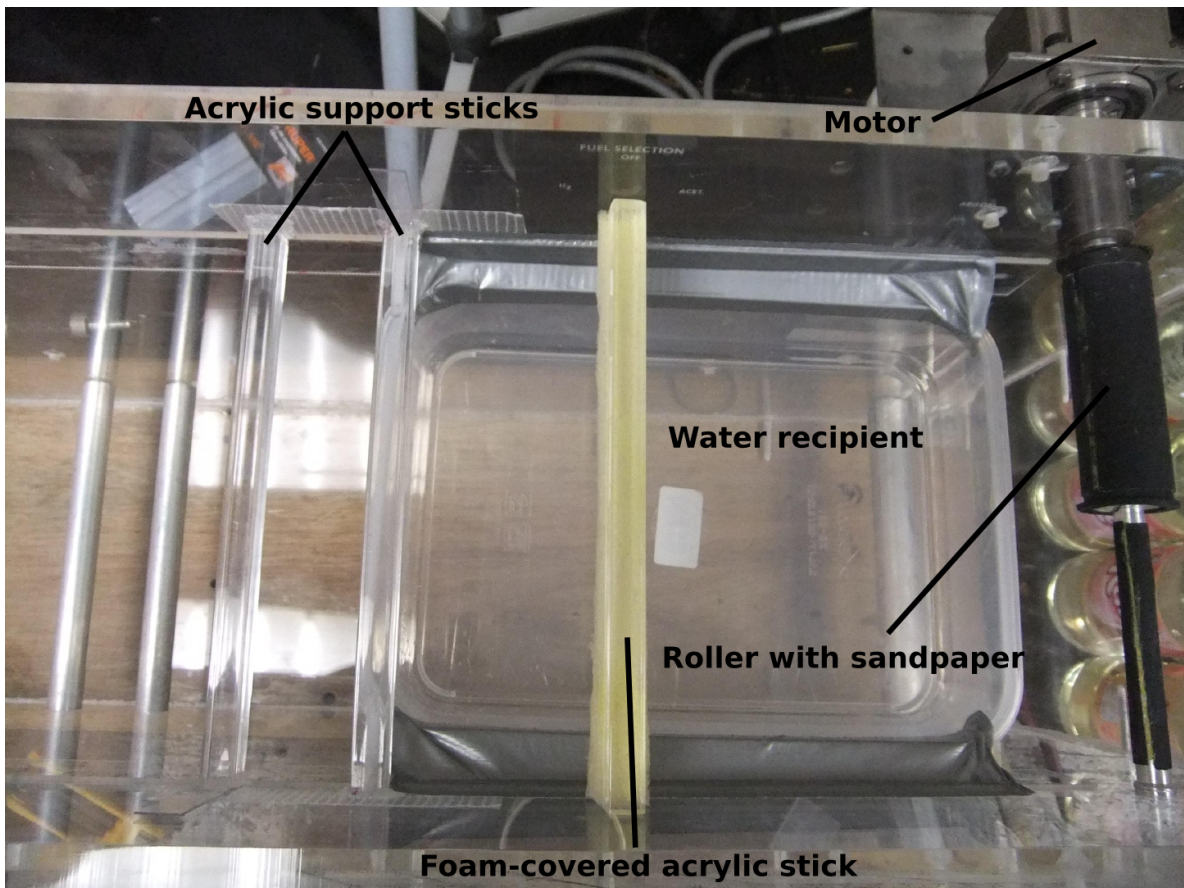


Figure 7: Top view of the tank showing the motor, roller, acrylic sticks and the cleaning station



Figure 8: Colored pasta beads of anchellini used to track down flow paths

dations are described in Sbalzarini & Koumoutsakos (2005). To work, the plug-in requires several pre-process stages such as image sharpening by applying a Gaussian filter, converting the RGB frames into grayscale images, etc. (see MOSAIC (2009) for details). In the second approach, I manually picked individual particles frame by frame as the high opacity of the syrup caused errors in the particle-tracking program. The automatic tracking was only used for shallow particles.

## II.1 Similarity and nondimensional analysis

One important aspect of laboratory experiments is whether the natural phenomenon of interest and the experimental model are similar. Buckingham's-II theorem is the basis to establish if an experiment is properly scaled. It warrants that two physical systems behave similarly when a series of dimensionless groups  $\Pi_i$  that define them have the same values. An important point is that two systems may have the same values of  $\Pi_i$  even if they are of different size. This is true even if the dimensional parameters  $P_N$ , that make up the  $\Pi_i$  groups, are very different. Moreover, dynamical similarity is a natural generalization part of Buckingham's-II theorem (geometric similitude is necessary, but not sufficient, condition for dynamical similarity).

Table II lists some important dimensionless numbers for geodynamic and fluid mechanics problems in general, some of which are discussed next. The Rayleigh number,  $Ra$ , characterizes the heat transfer in a fluid by comparing the thermal buoyancy forces to the thermal diffusion and viscous dissipation (Bercovici, 2009). The Prandtl number,  $Pr$ , the ratio of momentum diffusivity (kinematic viscosity) to thermal diffusivity.  $Pr$  is a physical attribute of the material and is flow independent. The ratio between  $Ra/Pr$  is called the Grashof number. This number can also be written as  $Va/\nu$  and

Table II: Units and parameters for mantle convection. Modified from Bercovici (2009); Fowler (2005) (page 53,556-558)

Dimensionless number	Notation	Functional relation	Physical parameter	Value for the mantle
Rayleigh	Ra	$\frac{\alpha \Delta T g a^3}{\nu \kappa}$	a = length $\alpha$ = expansivity $\Delta T$ = temperature difference g = gravitational acceleration $\nu$ = kinematic viscosity $\kappa$ = thermal diffusivity	$4.2 \times 10^7$
Prandtl	Pr	$\frac{C_p \eta}{k}$	$C_p$ = heat capacity $\eta$ = dynamic viscosity k = heat conductivity	$3.3 \times 10^{23}$
Grashof	Gr	$\frac{\alpha \Delta T g a^3}{\nu^2}$	a = length $\Delta T$ = temperature difference g = gravitational acceleration $\alpha$ = expansivity $\nu$ = kinematic viscosity	$1.3 \times 10^{-15}$
Reynolds	Re	$\frac{V a}{\nu}$	a = length V = flow velocity $\nu$ = kinematic viscosity	$7 \times 10^{-20}$
Euler	Eu	$\frac{\Delta P}{\rho V^2}$	$\Delta P$ = pressure difference V = flow velocity $\rho$ = density	$1.5 \times 10^{19}$
Péclet	Pe	$\frac{V d}{\kappa}$	d = tectonic plate thickness V = flow velocity $\kappa$ = thermal diffusivity	$1.0 \times 10^3$

is called the Reynolds number  $Re$  (see Table II for its definition). When performing a nondimensionalization the Reynolds number is a more natural choice to use than the Grashof number. Finally, the Reynolds  $Re$  number measures the ratio of inertial forces to viscous force and represents whether the flow is laminar or turbulent.

The analogue model used here is isothermal. Thus, the only relevant nondimensional group is the Reynolds number and dynamical similarity is guaranteed if  $Re$  is the same for both natural subduction and tank. In the case of the subduction tank  $Re$  is  $\sim 10^{-7}$ . By contrast in the case of subduction in the Earth's mantle  $Re$  is  $\sim 10^{-20}$  (Table II). Clearly, the analog model is not properly scaled. However, the achieving of strict similarity is impractical. That requires the use of a material with the consistency of pitch ( $10^7 \text{ Pa} \cdot \text{s}$ ) or reduce the speed to such a degree that it would take years to complete the experiments. Even though strict dynamic similarity is not achieved in the experiments, it can be demonstrated that a sufficiently small  $Re$  is enough to ensure it. To illustrate this, consider the Navier-Stokes equations and the equation of continuity.

$$\left( \frac{\partial u}{\partial t} + u \frac{\partial u}{\partial x} + v \frac{\partial u}{\partial y} \right) = -\frac{1}{\rho} \frac{\partial P}{\partial x} + \nu \left( \frac{\partial^2 u}{\partial x^2} + \frac{\partial^2 u}{\partial y^2} \right); \quad (1)$$

$$\left( \frac{\partial v}{\partial t} + u \frac{\partial v}{\partial x} + v \frac{\partial v}{\partial y} \right) = -\frac{1}{\rho} \frac{\partial P}{\partial y} + \nu \left( \frac{\partial^2 v}{\partial x^2} + \frac{\partial^2 v}{\partial y^2} \right); \quad (2)$$

$$\frac{\partial u}{\partial x} + \frac{\partial v}{\partial y} = 0. \quad (3)$$

These equations describe the motion of an incompressible fluid substance. In equations (1)-(3)  $\nu$  is the kinematic viscosity,  $P$  is the fluid pressure, and  $v$  and  $u$  are the  $x$  and  $y$  components of the fluid's velocity, respectively. For simplicity I considered a two dimensional flow. Now lets express the involved variables in the following way:  $x = Lx'$ ,  $y = Ly'$ ,  $u = Vu'$ ,  $v = Vv'$ ,  $P = P_\infty + (P_0 - P_\infty)P'$ , and  $t = \frac{L}{V}t'$ , where  $L, V, P_0, P_\infty$  are

the characteristic length, velocity, and pressures involved in the problem, respectively. Also note that equations variables are expressed in terms of nondimensional quantities  $x', y', u', v'$ , and  $t'$ . Substituting those relations in equations (1)-(3) and factoring terms we obtain:

$$Re \left( \frac{\partial u'}{\partial t'} + u' \frac{\partial u'}{\partial x'} + v' \frac{\partial u'}{\partial y'} \right) = ReEu \frac{\partial P'}{\partial x'} - \left( \frac{\partial^2 u'}{\partial x'^2} + \frac{\partial^2 u'}{\partial y'^2} \right); \quad (4)$$

$$Re \left( \frac{\partial v'}{\partial t'} + u' \frac{\partial v'}{\partial x'} + v' \frac{\partial v'}{\partial y'} \right) = ReEu \frac{\partial P'}{\partial y'} - \left( \frac{\partial^2 v'}{\partial x'^2} + \frac{\partial^2 v'}{\partial y'^2} \right); \quad (5)$$

$$\frac{\partial u'}{\partial x'} + \frac{\partial v'}{\partial y'} = 0. \quad (6)$$

Finally, it can be seen that for a sufficiently small  $Re$  the solution is independent of time and pressure. Moreover, the solution is independent of the viscosity and the solution, only depends on the boundary conditions. Consequently, only geometric similarity is required for systems with small Reynolds numbers. If we assume that the tank, with its 17 cm-thick layer of corn syrup, is representative of convection in the upper mantle (700 km-thick), then the experiment is scaled at a ratio of 1:40,000,000. Based on this ratio and considering the values of gravity, density, and viscosity shown in Table III, a characteristic experimental velocity of 185 mm/min can be obtained for the laboratory setup (see calculation details in Table III). This velocity is equivalent to a subduction rate of 10 cm/yr in nature (Table III). These results indicate that subduction in the analog model proceeds at a rate of 4 cm/yr and 1.4 cm/yr for the fast and slow strip, respectively. In other words, subduction in the experimental setup is 66% slower than the modern subduction rate observed in the northern MASZ (Table I).

Table III: Scaling parameters in nature and the laboratory model. Modified from (Brydson, 1999; Heuret *et al.*, 2007; Bercovici, 2009) (page 400,478,53)

Parameter	Nature	Scaled model
Gravitational acceleration (g) $\text{m s}^{-2}$	9.81	9.81
Thickness, (m)		
$H$ , upper mantle	700.000	0.17
Scale factor for length	$L_{model}/L_{nature} = 2.4 \times 10^{-7}$	
Density, ( $\text{kg} \times \text{m}^{-3}$ )		
$\rho_c$ , continental lithosphere	3140	1180
$\rho_m$ , upper mantle	3220	1353
Density contrast ( $\rho_c - \rho_m$ )	-80	-173
Viscosity, ( $\text{Pa} \times \text{s}$ )		
$\eta_c$ , continental lithosphere	$10^{24}$	
$\eta_m$ , upper mantle	$5 \times 10^{19}$	6.5
Characteristic time, (s)	$2.5 \times 10^{14} \text{s}$ ( $\sim 8 \text{ Myr}$ )	60s (1 min)
$\frac{t_{nature}}{t_{model}} = \frac{(\Delta\rho g H)_{model}}{(\Delta\rho g H)_{nature}} \times \frac{\eta_{nature}}{\eta_{model}}$		
Characteristic velocity,	10 cm/yr	185 mm/min
$\frac{V_{nature}}{V_{model}} = \frac{(L_{nature} \times t_{model})}{(L_{model} \times t_{nature})}$		
Rivera plate velocity	$\sim 2 \text{ cm/yr}$	1.4 cm/yr
Cocos plate velocity	$\sim 5 \text{ cm/yr}$	4 cm/yr

## II.2 Model limits

Even though the model captures the physics of the MASZ, it is a simplified representation of the actual phenomenon. Some of its limitations are the following. For example, the model does not have any internal heat sources. Furthermore, the strips span the whole width of the tank therefore no flow at the tank's boundaries occurs. In addition, the strips form a conveyor belt. Thus at the lower part of the tank, where the strips make a sharp return, the flow does not conform to the natural process in which slabs sink into the deep mantle.

Another limitation is that the gap appears at a depth between 60 and ~200 km. In the experiment the two strips are continuously separated along their track. As the strips share the same roller, only velocities with reason 1:3 can be realized. Neither the strips nor the acrylic plate deform in any way during the experiment. In reality, both the continental crust and the mantle are coupled via viscous drag (Contreras, 2012), causing brittle failure of the volcanic arc (Suter *et al.*, 2001; Ferrari & Rosas-Elguera, 1999).

## Chapter III

### Results

Six experiments were performed (details are presented in Table IV); two of them were recorded with the camera placed above the tank looking down the z-axis; four of them were recorded with the camera placed on the side of the tank looking down the y-axis (Fig. 5). Each experiment had different particle arrangement and were designed to bring to light flow patterns in different regions. In all the experiments an acrylic plate was placed on top of the syrup and floated on it for the duration of the observations. Additionally the dip of the slabs is the same for all experiments.

Table IV: List of experiments and their set up

Experiment	Camera position	Recording duration (min)	Motor velocity (mm/min)	Particle arrangement
1	top view	5:54	50	Particles are located at the interface between acrylic plate and syrup
2	top view	11:45	50	Particles are located at a depth of 2-7 cm, mean 4 cm in the syrup
3	side view	17:40	50	Particles are located at a depth of 2-5 cm, mean 3 cm in the syrup
4	side view	14:05	50	Particles are located at a depth of 2-6 cm, mean 3 cm in the syrup
5	side view	16:34	50	Particles are located at a depth of 1-5 cm, mean 2 cm in the syrup
6	side view	13:40	50	Particles are located at a depth of 2-7 cm, mean 4 cm in the syrup

Experiment's results are plotted in pixels and their relation to the natural scale is as follows: 100 km : 120 px for images in the “xy” plane and 100 km : 150 px for images in the “xz” plane. As a further reference plots include the locations of the TMVB as a white bar and the location of the city of Guadalajara. Plots in “xy” plane also include the location of the trench, the scaled velocities of the strips and the gap between the

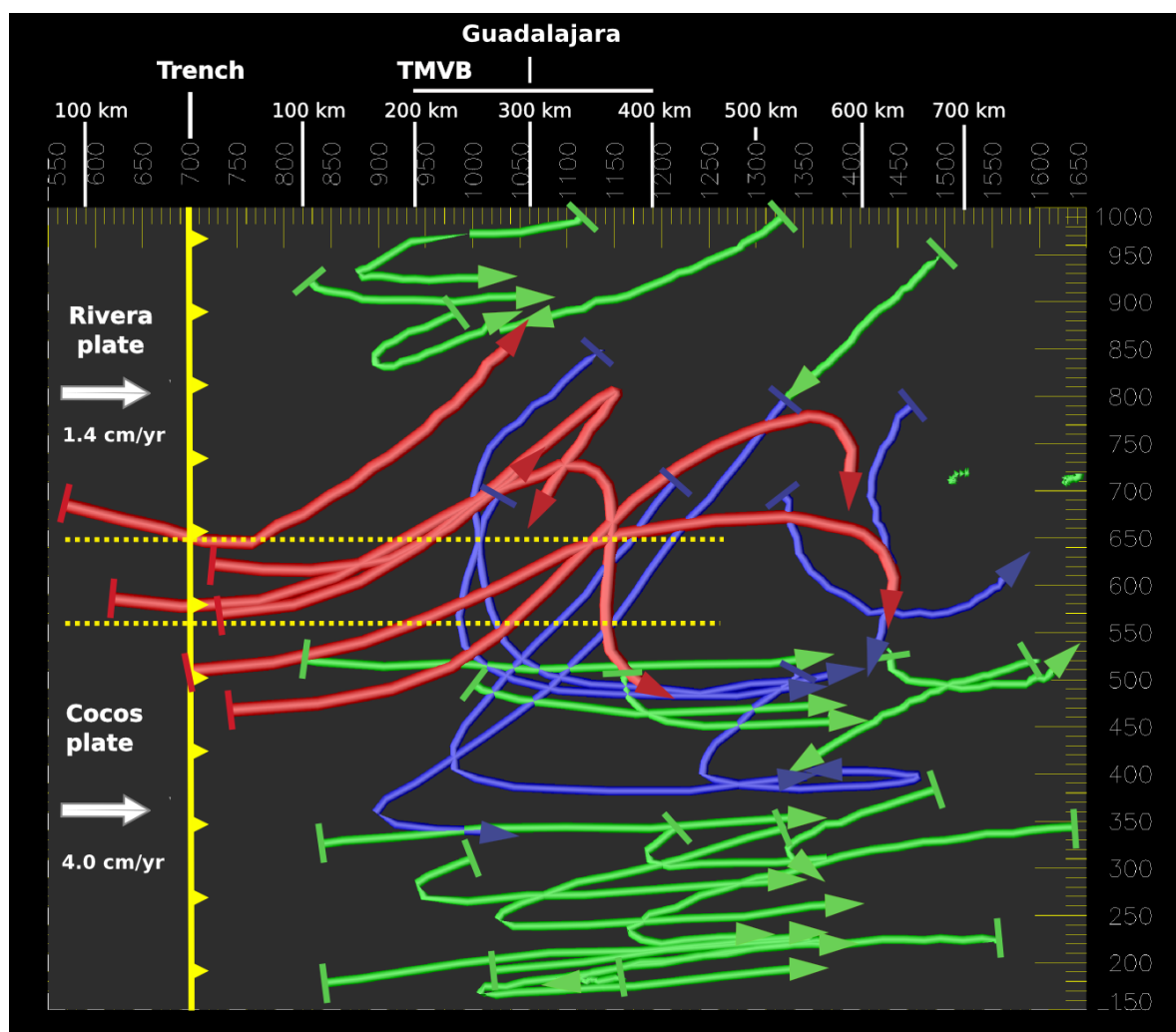


Figure 9: Top view of the flow patterns in the mantle wedge of the simulated subduction zone. Pathlines are for particles at depths between 2cm - 7cm. White arrows show velocity during the experiment whereas black marking start points of particles. Yellow solid line marks the trench along the tank and dashed lines represent the gap between the two strips. Bars mark the initial position of the markers (pasta beads). Arrows indicate the final position of the markers. See test for further details of the experiment.

plates (dashed lines).

The starting point of each particle is marked by a solid bar and the end is represented by an arrow. Figure 9 corresponds to pathlines of particles at a depth between 2-7 cm, mean depth of  $\sim 4$  cm (see experiment 2 in Table IV). Colors highlight to three different particle movements. Green paths are for those particles in the mantle wedge with a motion strongly directed toward the trench, never crossing the gap between the two plates. Green color also was used for fast downgoing particles attached to the strips. Blue ones are for those particles in the mantle wedge whose movements are strongly

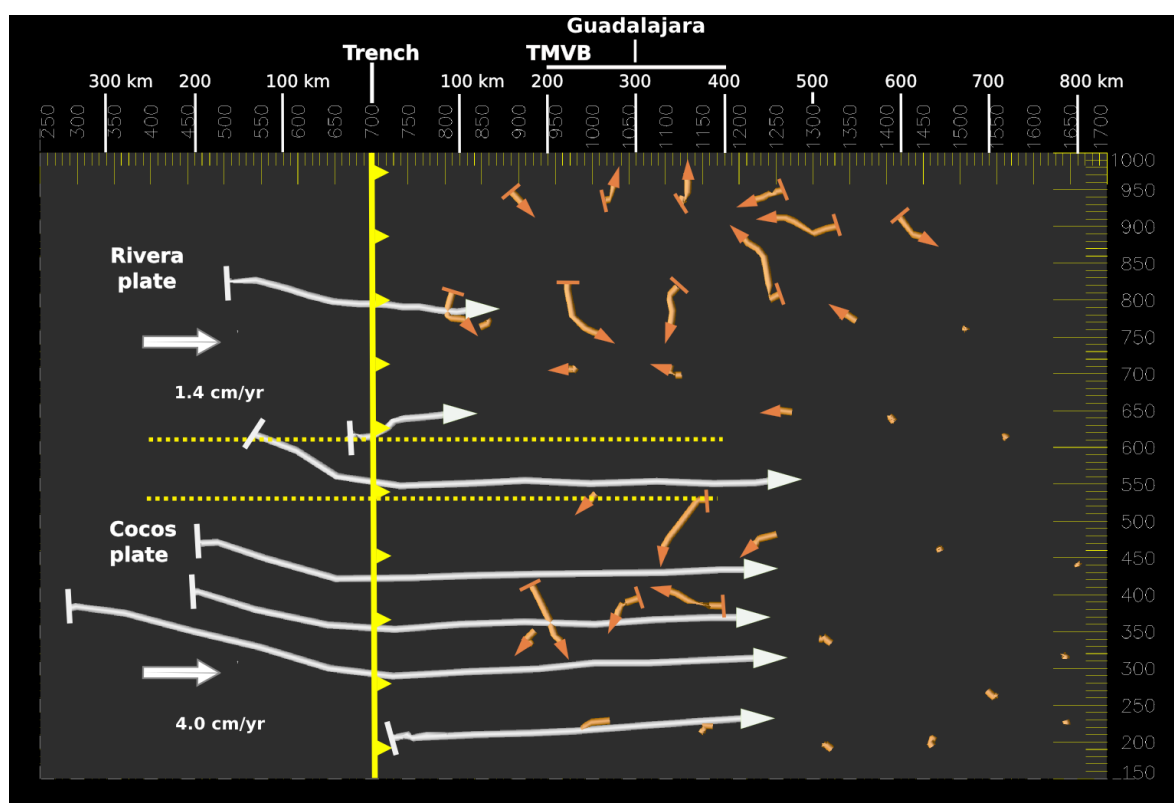


Figure 10: Top view of the flow patterns in the mantle wedge of the simulated subduction zone. Pathlines are for particles situated on the top of the syrup. White arrows show velocity during the experiment whereas black marking start points of particles. Yellow solid line marks the trench along the tank and dashed lines represent the gap between the two strips. Bars mark the initial position of the markers (pasta beads). Arrows indicate the final position of the markers. See text for further details of the experiment.

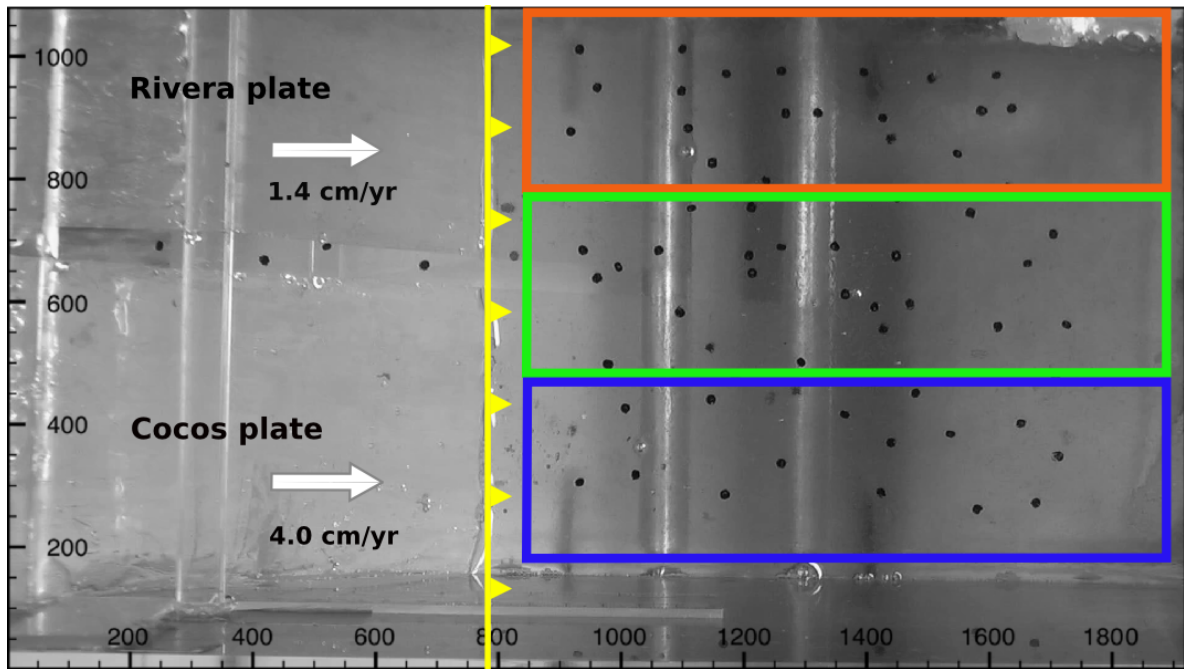


Figure 11: Top view of the experimental tank. Black points are material markers (inked anchelini pasta). Yellow solid line indicates the trench, arrows the experimental plates velocities (cm/yr). The colored rectangle represent the Rivera plate (orange), the gap (green) and the Cocos plate (blue). Scale is in pixels

vertical, crossing the gap between the two strips. Some of them go down with the strip as well. Red pathlines are for particles originating in the asthenospheric mantle and entering the mantle wedge through the gap. After entering the gap they reach a depth where they stop, change their direction and move towards the fast strip and ascend into the mantle wedge (Fig. 9).

Figure 10 (see experiment 1 in Table IV) corresponds to particles situated on the top of the syrup near the floating acrylic plate. White pathlines show flows from the asthenospheric mantle reaching the trench and go down with the strips in the lower part of the syrup. Orange-colored pathlines correspond to particles within the mantle wedge. As can be appreciated in Figure 10, they show no specific pattern nor a general direction of the flow.

Figures 13 through 19 incorporate the results of four different experiments (see details in Table IV) recorded in the “xz” plane. The yellow dashed line marks the location of the acrylic plate simulating the continental crust. The yellow solid lines indicate the polyethylene strips simulating the subducting plates.

Orange pathlines are for particles in the mantle wedge of the Rivera plate, green pathlines for particles at the gap and blue ones for particles in the mantle wedge of the Cocos plate (Fig. 11). For the Rivera plate, particles move towards the trench and go down with the strip (Fig. 13).

Notice that in this figure two sets of particles have been labeled “a” and “b”. Those labeled “a” move in the distinctive pattern expected for subduction zones: they flow toward the trench and go down with the subducting slab. Those labeled “b”, by

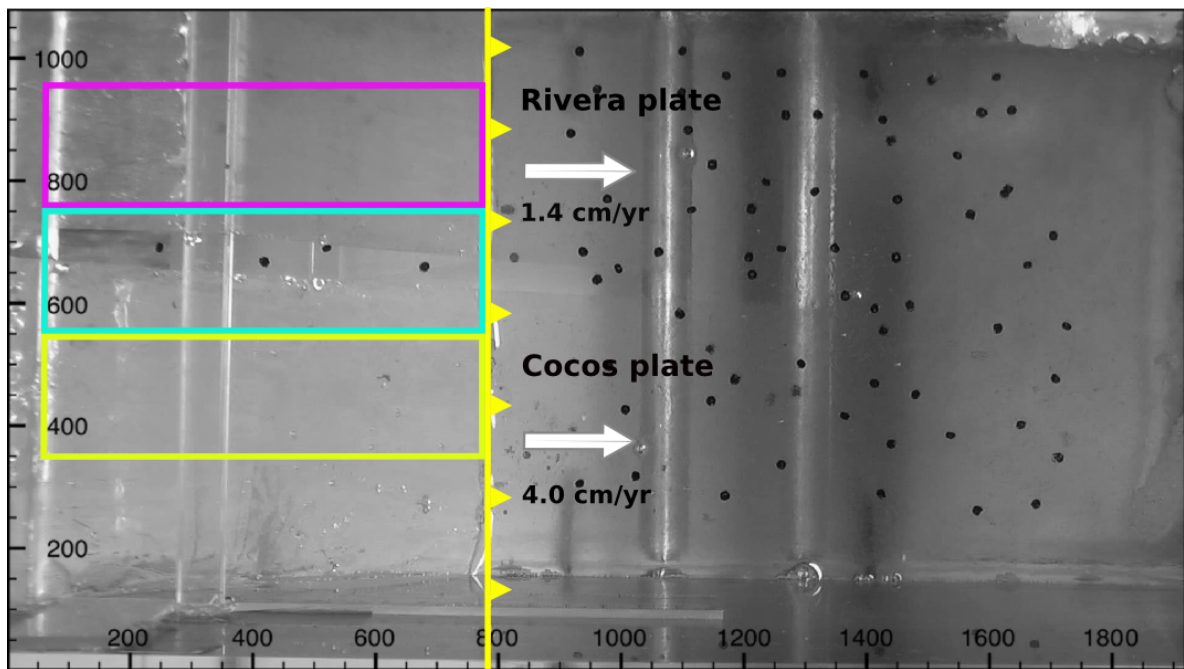


Figure 12: Top view of the experimental tank. Black points are material markers (inked anchelini pasta). Yellow solid line indicates the trench, arrows the experimental plates velocities (cm/yr). The colored rectangle represent the Rivera plate (orange), the gap (green) and the Cocos plate (blue). Scale is in pixels

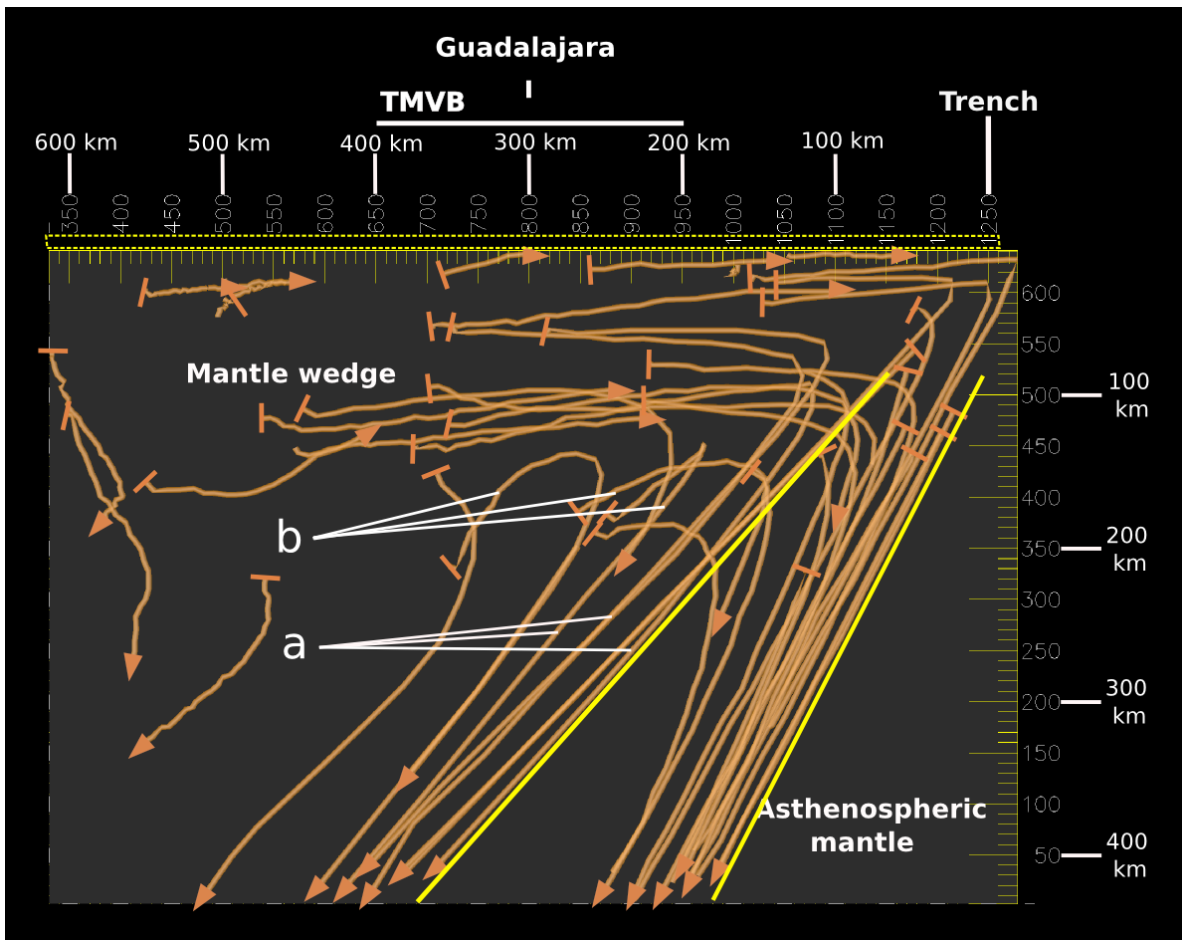


Figure 13: Flow patterns in the mantle wedge above the Rivera plate revealed by the analog experiment. The dashed yellow line shows the location of the acrylic plate representing the continental crust of the North America plate. The white solid line on the top corresponds to the location of the Trans Mexican Volcanic Belt (TMVB) and the city of Guadalajara. Axes are in pixels. Yellow solid lines indicate the location of the subducting slabs.

contrast, have a strong upward movement before they are dragged down by the down-draft of the slab.

Particles near the gap between the two plates (Fig. 14) display pathlines that move horizontally towards the strip; then the particles go down with the simulated Cocos plate. Finally, Figure 15 presents the pathlines described by particles in the mantle wedge above the Cocos plate (Fig. 11). In Figure 15 the particles in the upper mantle

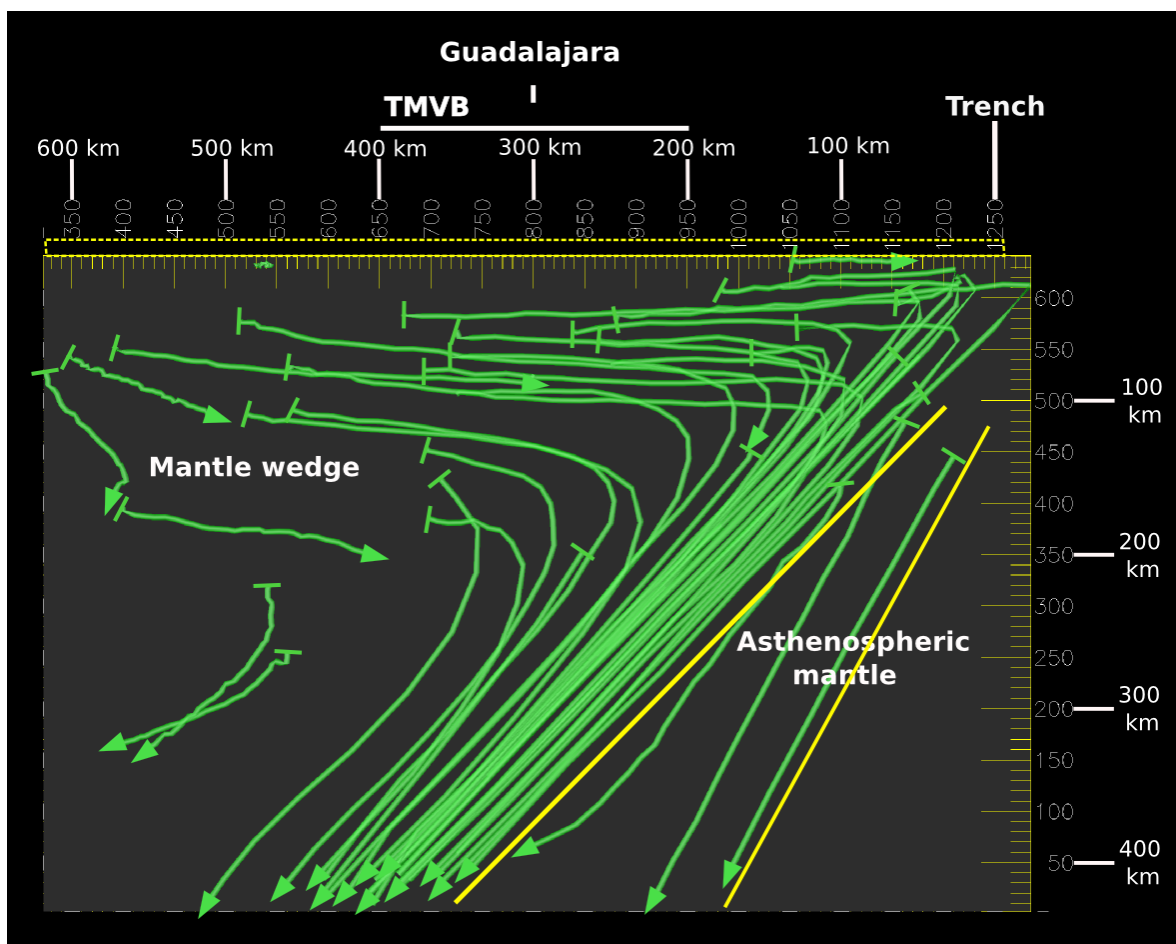


Figure 14: Flow patterns in the mantle wedge above the gap between Rivera and Cocos plates revealed by the analog experiment. The dashed yellow line shows the location of the acrylic plate representing the continental crust of the North America plate. The white solid line on the top corresponds to the location of the Trans Mexican Volcanic Belt (TMVB) and the city of Guadalajara. Axes are in pixels. Yellow solid lines indicate the location of the subducting slabs.

wedge move horizontally towards the plate and then go down, whereas particles in the lower part present a downward movement parallel to the sinking strip. Notice that particles within the simulated Rivera mantle wedge (Fig. 13) tend to move towards the Cocos plate. Additionally notice that, particles situated in the Cocos mantle wedge tend to move towards the strip and then are dragged downwards.

Now, Figures 16 - 18 present the flowlines within the simulated asthenospheric man-

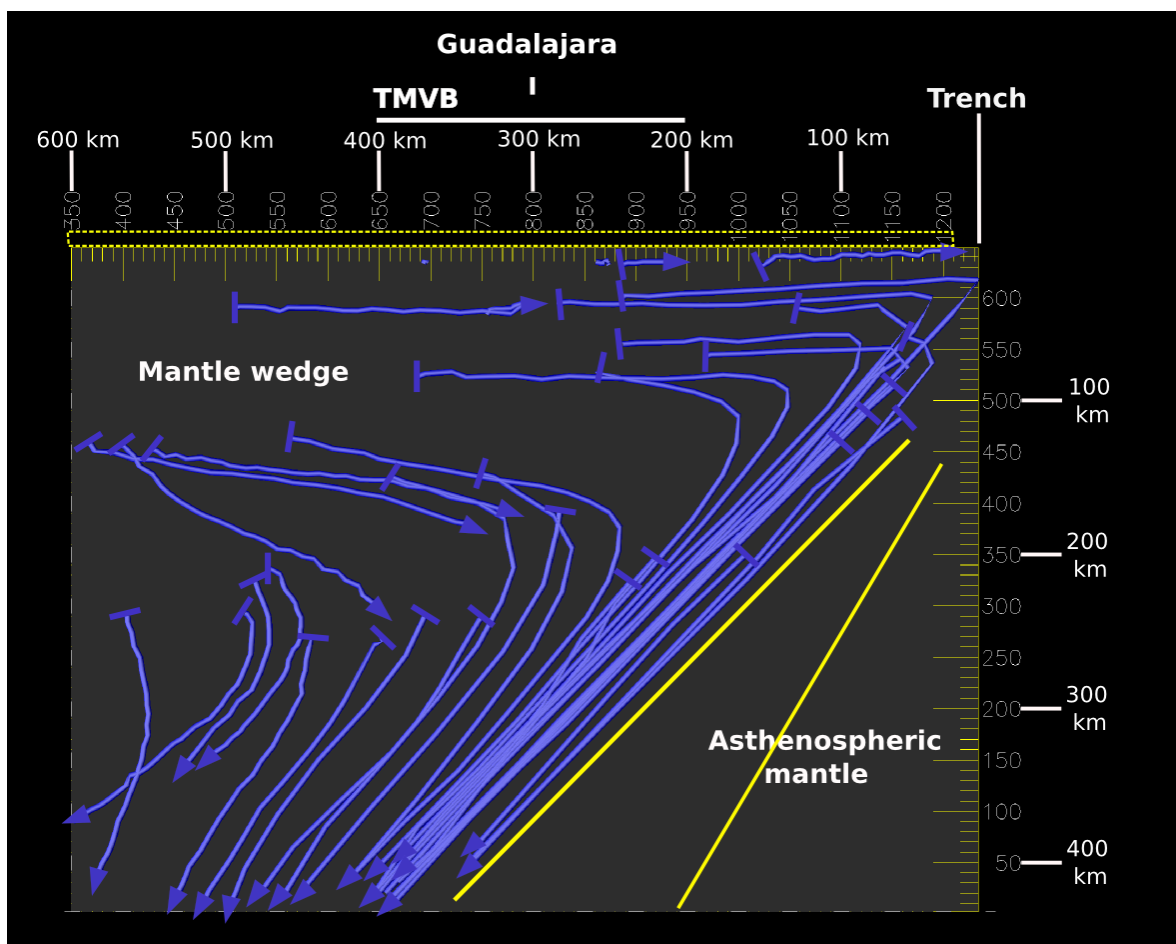


Figure 15: Flow patterns in the mantle wedge above the Cocos plate revealed by the analog experiment. The dashed yellow line shows the location of the acrylic plate representing the continental crust of the North America plate. The white solid line on the top corresponds to the location of the Trans Mexican Volcanic Belt (TMVB) and the city of Guadalajara. Axes are in pixels. Yellow solid lines indicate the location of the subducting slabs.

tle. Those were also divided into three areas (colored rectangles in Fig. 12). Magenta represents pathlines for the Rivera plate, cyan ones for the gap and yellow pathlines for the Cocos plate. All particles located at the modeled Rivera plate (Fig. 16) show movements towards the sinking plate. However, the plot includes one that go down with the Cocos plate and another one passes through the gap between the two plates. Also note that particles were caught in the retrograde flow of the conveyor belt at the bottom

of the tank. The gap area (Fig. 17) show similar patterns as in the prior figure. The gap region, however, contains the majority of particles which enter the mantle wedge. The asthenospheric mantle corresponding to the Cocos plate contains the particle with major ascend into the mantle wedge (Fig. 18).

Figure 19 combines the results from the mantle wedge and the asthenospheric mantle in the “xz” plane. Colors of pathlines in the mantle wedge are as in prior figures can be observed that poloidal flow is dominant in the mantle wedge. Flowlines within the asthenospheric mantle appear in different colors for presentation reasons. It can be observed that poloidal flow is dominant for the mantle wedge. White paths are for those particles that are dragged down with the strips, the purple ones show retrograde

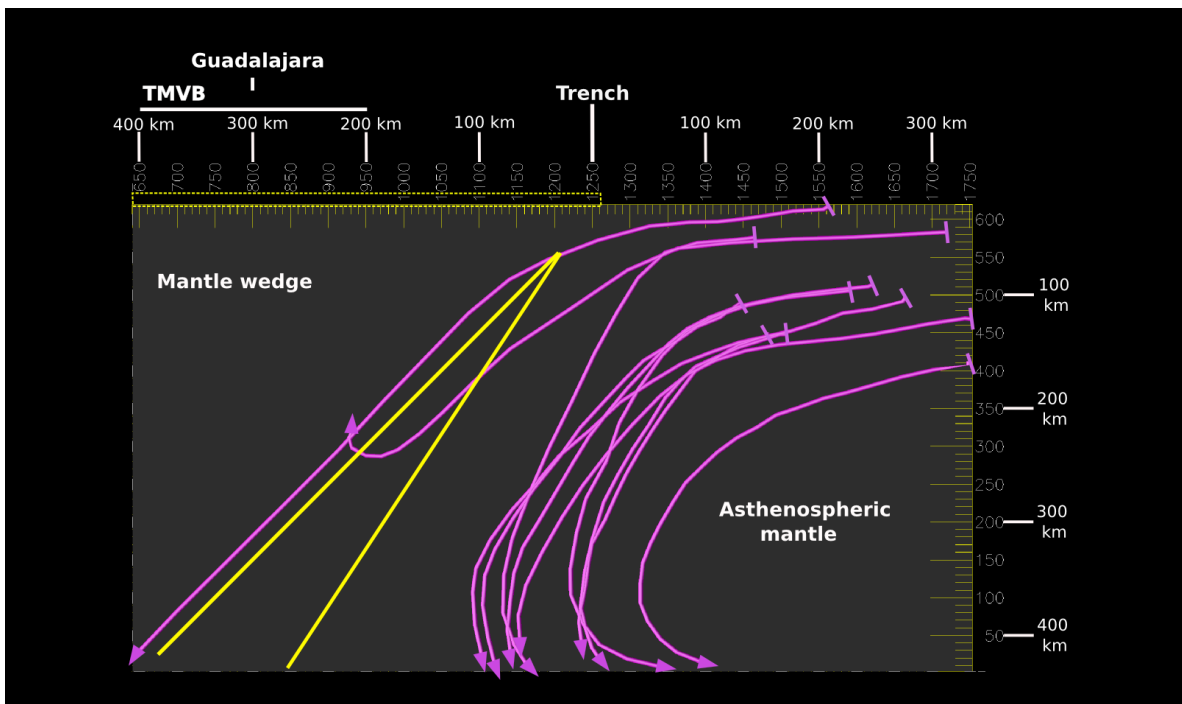


Figure 16: Flow patterns in the asthenospheric mantle above the Rivera plate revealed by the analog experiment. The dashed yellow line shows the location of the acrylic plate representing the continental crust of the North America plate. The white solid line on the top corresponds to the location of the Trans Mexican Volcanic Belt (TMVB) and the city of Guadalajara. Axes are in pixels. Yellow solid lines indicate the location of the subducting slabs.

movement and the red pathlines are for particles entering through the gap into the mantle wedge and ascending under the volcanic arc. Notice that red pathlines after entering and ascending into the mantle wedge appear to be continuous with flowlines in the mantle wedge. This is, orange pathlines in the mantle wedge are continuations of red pathlines entering through the gap. Furthermore, the red pathlines with mayor ascend could be continued with pathlines located in the upper part of the tank.

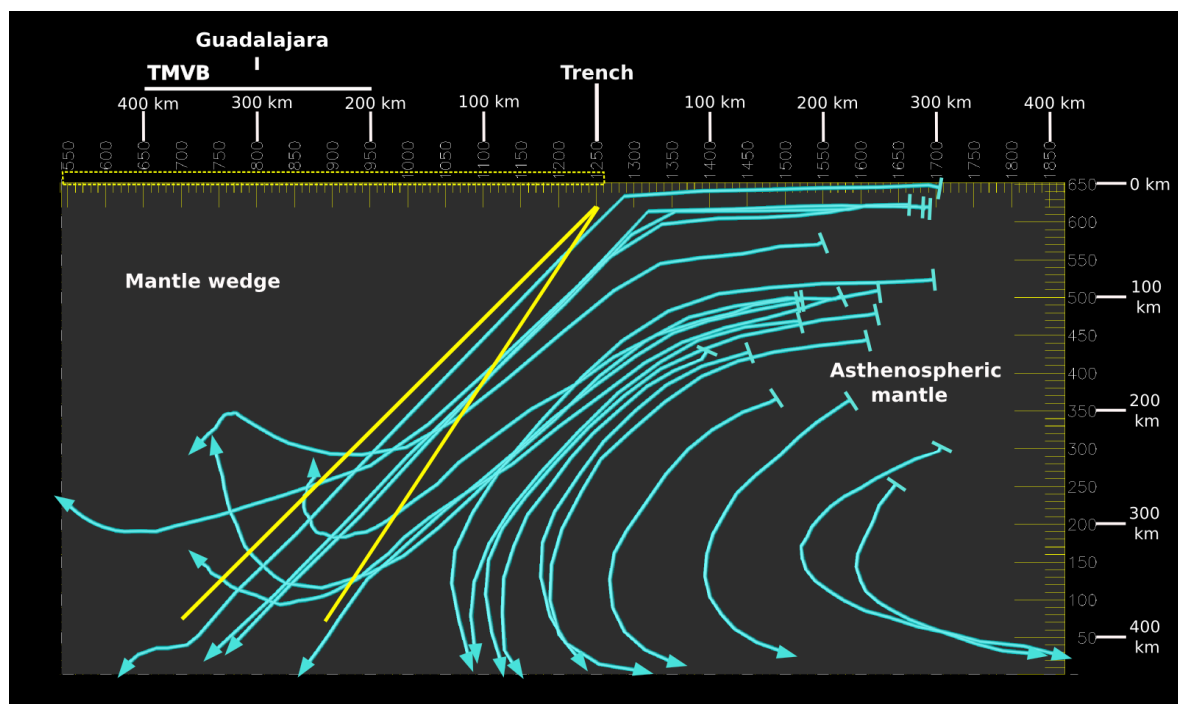


Figure 17: Flow patterns in the asthenospheric mantle above the gap between the Rivera and Cocos plates revealed by the analog experiment. The dashed yellow line shows the location of the acrylic plate representing the continental crust of the North America plate. The white solid line on the top corresponds to the location of the Trans Mexican Volcanic Belt (TMVB) and the city of Guadalajara. Axes are in pixels. Yellow solid lines indicate the location of the subducting slabs.

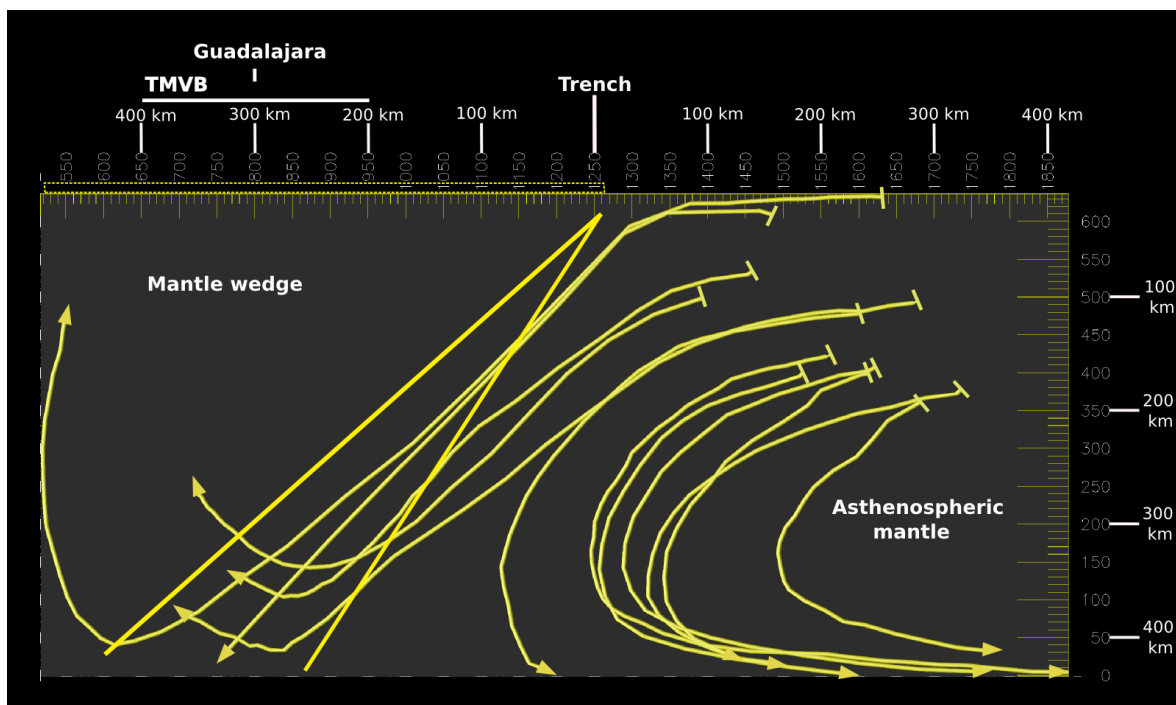


Figure 18: Flow patterns in the asthenospheric mantle above the Cocos plate revealed by the analog experiment. The dashed yellow line shows the location of the acrylic plate representing the continental crust of the North America plate. The white solid line on the top corresponds to the location of the Trans Mexican Volcanic Belt (TMVB) and the city of Guadalajara. Axes are in pixels. Yellow solid lines indicate the location of the subducting slabs.

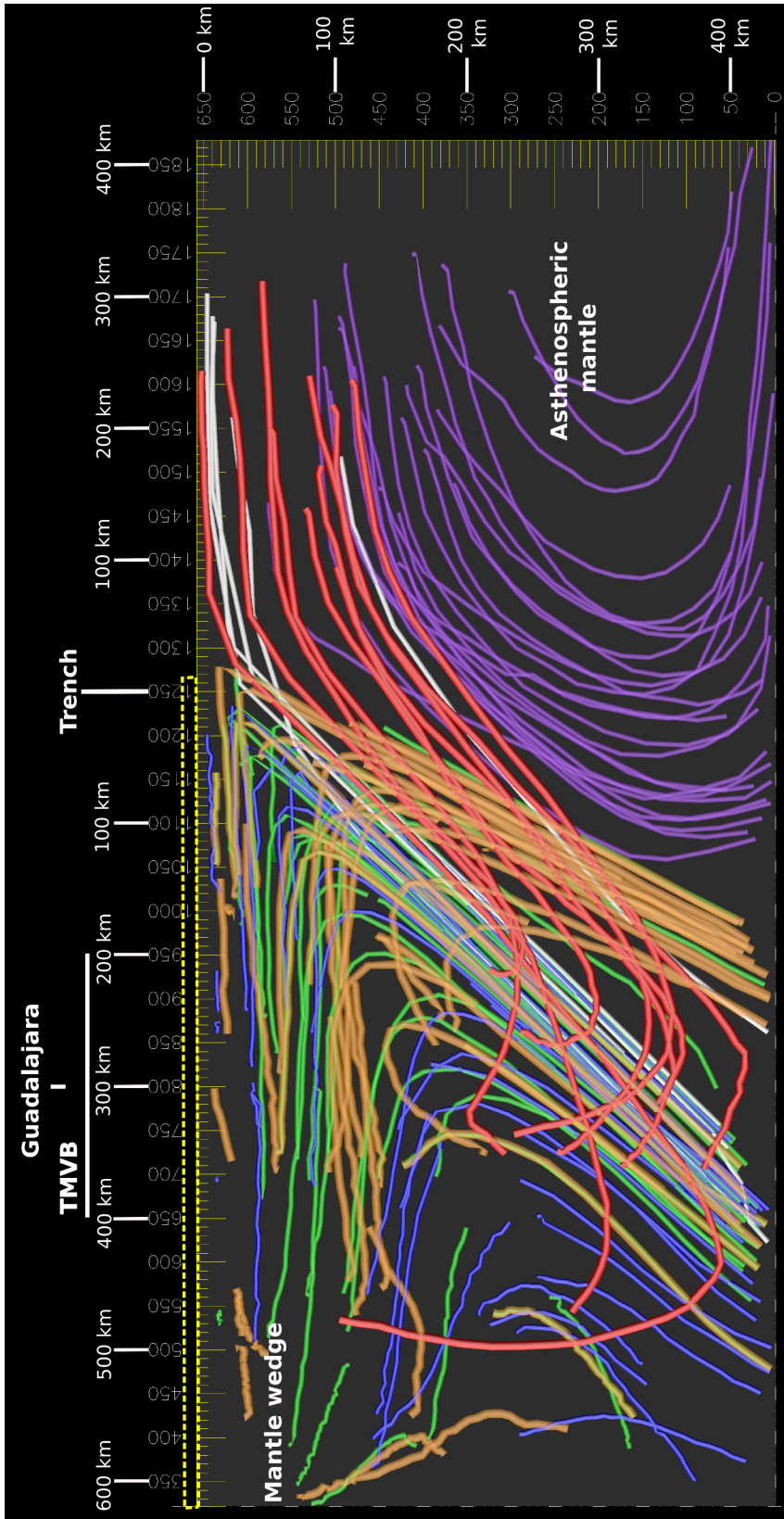


Figure 19: Merged results plotting asthenospheric mantle and mantle wedge paths. Colors are indicating the different flow paths. The acrylic plate (yellow dashed line) and the corrected (red line) TMVB location and the city of Guadalajara. Axes are in pixels as well as their relation to km.

## Chapter IV

### Discussion

As stated earlier, the analog model presented here is best suited for a tectonic configuration in which the gap between the Rivera and Cocos slabs is located at a shallow depth. Indeed, recent results by Perez-Ramirez *et al.* (2012) indicate that this may be the case and that the gap is located at a depth of 60 km. However, there are other tomography studies that seem to suggest that the gap is located at a depth of 200 km (Fig. 3). If that were the case, then model results would need to be shifted  $\sim 150$  km inland to account for the location of the gap under the forearc. Thus, the hydraulic jump would be located in the northern terminus of the TMVB, rather than directly under it.

The 3D-analog modeling used here has been presented in previous works (Chemenda *et al.*, 2001; Schellart, 2004; Heuret *et al.*, 2007). These works present similar experimental set-ups where a simulated oceanic lithosphere is forced to subduct into water or syrup representing the upper mantle. The forcing used to initiate the subduction process is achieved by pistons, pushing the subducted plate against an overriding plate or simply depressing a floating simulated oceanic plate at the edge. The model I present here, differs from prior ones in that it uses a conveyor belt to simulate the oceanic plate subduction. Besides, the model uses two different plates, angles and velocities to simulate the complex subduction of the MASZ. Therefore, rollback-induced flow beneath the slab (Schellart, 2004) is not taken into account. Nevertheless, the resulting poloidal flow in the simulated mantle wedge is in agreement with those observed by

Schellart (2004). Pathlines as seen in Figures 13 through 19 indicates a flow induced by motion of the subducting plate. Moreover, as seen in Figure 9, mantle wedge material is sucked from the low velocity plate to the fast plate. This results from the fact that the fast plate transports more material into the lower mantle and material is replaced by an inflow from the slow plate.

At the same time, the model has clear limitations. For example, the asthenospheric mantle has clear non-realistic boundary effects. This can be appreciated in the purple pathlines in Figure 19: they show the influence of the strip moving backwards.

A new result coming out from the analog experiments presented here is the presence of a strong poloidal flow around the gap separating the slabs. This flow is imaged by the pathlines of particles entering the mantle wedge through the gap between the strips (red pathlines in Fig. 19). This flow pattern can be explained in terms of a physical phenomenon known as hydraulic jump. It is observed when a rapid flow enters a low velocity zone and an abrupt ascend occurs. The physical explanation is that the rapid flow has a high kinetic energy, which decreases entering the slower flow and converts it into potential energy, leading the fluid to rise. The implications of this phenomenon are two fold: on one hand, it introduces material from the asthenospheric mantle into the mantle wedge and, on the other hand, deep mantle material is transported into shallower regions of the wedge. Therefore, slab rollback and slab detachment may not be the cause for hot and less dense material entering the mantle wedge through the gap as has been proposed by Ferrari *et al.* (2012) and Ferrari (2004).

In this regard, those authors have suggested that the presence of oceanic-island basalts (OIB) in the western TMVB is the result of chemically-enriched asthenospheric mantle entering into the mantle wedge through the slab gap. Furthermore, Gómez-

Tuena *et al.* (2007) has suggested that the different magma types of the TMVB must have originated from a heterogeneous mantle wedge. A heterogeneous mantle, according to these authors, not necessarily refers to a mixture of different mantle compositions. It can refer to different degrees of hydration in the mantle. The model, is consistent with those ideas and as it provides with the mechanism (hydraulic jump) by which hot subslab material (possibly enriched) enters into mantle wedge and gives an explanation to the intraplate volcanism.

Another feature of the seismic tomography is the presence of a low velocity anomaly under the western TMVB and Los Altos de Jalisco region (Fig. 3). Often, these anomalies are thought to reveal hot, low density mantle. The flowlines observed in the analog model (Fig. 19) demonstrate that indeed deep, hot mantle may be transported into the mantle wedge, ascending at the northern edge of the TMVB. Furthermore, this observations agrees with the heat flow maps of Manea & Manea (2011). The heat flow map produced by these authors for southern Mexico show high values for the back arc as well as for the Altos de Jalisco region. Furthermore, experiment results provide with an explanation as to why the anomalous low velocity mantle shifts its position to the east (Fig. 3). The model suggests that after new astenospheric material enters through the gap between the slab, flow is directed through the fast slab, advecting heat in an eastward direction.

Finally, the flow patterns obtained in this work are in agreement with seismic anisotropy observed for the Jalisco and Michoacan blocks (Soto *et al.*, 2009) and with results obtained by Schellart (2004). It can be appreciated in Figure 4 that the direction of the polarization plane of the fast ray under the Jalisco block is oblique with respect to the convergence vector. The analog experiments develop a similar pattern to that imaged by the anisotropy. Now, the anisotropy obtained by Soto *et al.* (2009) has

good coverage for the Rivera slab but lacks resolution for the Cocos slab. In this case the anisotropy results from Stubailo *et al.* (2012) were used to compare them with our results for the western Cocos plate. Anisotropy reveals that fast directions are normal to the trench, which are in accordance with the corner flow observed in the experiment. Caution should be exercised, however, as the complexity of the MASZ makes it difficult to locate exactly where the anisotropy is originating. The anisotropy may be located in the slab or even in the subslab mantle.

## Conclusions

Mantle flow beneath the Jalisco and Michoacan block has been studied using a simple model that takes into account differences in subducting angles and velocities observed in the western part of the MASZ. Experiments reveal the presence of poloidal and toroidal flows in the mantle wedge below those tectonic blocks. Furthermore, toroidal flow occur at two different depths. One at shallow depth where pathlines move towards the Cocos plate. In the second one, pathlines enter at deeper levels of the mantle wedge from the astenospheric mantle. The later flow implies that hot, less dense material is entering the mantle wedge and may explain the heterogeneous compositions of lavas erupted in the TMVB. Model results are also in agreement with seismic anisotropy observed in the western TMVB. Finally, the model provides with a consistent explanation of the high heat flow documented in the Los Altos de Jalisco area, in the back arc of the TMVB.

## References

- ALLAN, J.F. 1986. Geology of the northern Colima and Zacoalco grabens, southwest Mexico: Late Cenozoic rifting in the Mexican volcanic belt. *Geological Society of America Bulletin*, **97**(4), 473–485.
- BERCOVICI, D. 2009. *Mantle Dynamics: Treatise on Geophysics*. Elsevier.
- BRYDSON, J.A. 1999. *Plastics materials*. Butterworth-Heinemann.
- CHEMENDA, A.I., YANG, R.-K., STEPHAN, J.-F., KONSTANTINOVSKAYA, E.A., & IVANOV, G.M. 2001. New results from physical modelling of arc-continent collision in Taiwan: evolutionary model. *Tectonophysics*, **333**(1-2), 159–178.
- CONTRERAS, J. 2012. A model for the state of brittle failure of the western Trans-Mexican Volcanic Belt. *International Geology Review*, **1-12**
- DEMETS, C., & TRAYLEN, S. 2000. Motion of the Rivera plate since 10 Ma relative to the Pacific and North American plates and the mantle. *Tectonophysics*, **318**(1-4), 119–159.
- FERRARI, L. 2004. Slab detachment control on mafic volcanic pulse and mantle heterogeneity in central Mexico. *Geology*, **32**(1), 77.
- FERRARI, L., & ROSAS-ELGUERA, J. 1999. Late Miocene to Quaternary extension at the northern boundary of the Jalisco block, western Mexico: The Tepic-Zacoalco rift revised. *Geological Society of America Special Paper*, **334**, 41–64.
- FERRARI, L., PETRONE, C.M., & FRANCALANCI, L. 2001. Generation of oceanic-island basalt-type volcanism in the western Trans-Mexican volcanic belt by slab rollback, asthenosphere infiltration, and variable flux melting. *Geology*, **29**(6), 507–510.
- FERRARI, L., OROZCO-ESQUIVEL, T., MANEA, V., & MANEA, M. 2012. The dynamic history of the Trans-Mexican Volcanic Belt and the Mexico subduction zone. *Tectonophysics*, **522-523**, 122–149.
- FOWLER, C. M. R. 2005. *The Solid Earth: an Introduction to Global Geophysics*. 2nd ed. Cambridge University Press.
- GARDINE, M.D., DOMINGUEZ, T., WEST, M.E., GRAND, S.P., & SUHARDJA, S.K. 2007. The deep seismic structure of Volcan de Colima, Mexico. *Page 02 of: AGU Spring Meeting Abstracts*, vol. 1.

- GÓMEZ-TUENA, A., OROZCO-ESQUIVEL, M.T., & FERRARI, L. 2007. Igneous petrogenesis of the Trans-Mexican volcanic belt. *Geological Society of America Special Papers*, **422**, 129–181.
- HEURET, A., FUNICIELLO, F., FACCENNA, C., & LALLEMAND, S. 2007. Plate kinematics, slab shape and back-arc stress: A comparison between laboratory models and current subduction zones. *Earth and Planetary Science Letters*, **256**(3-4), 473–483.
- LONSDALE, P. 2005. Creation of the Cocos and Nazca plates by fission of the Farallon plate. *Tectonophysics*, **404**(3-4), 237–264.
- LUHR, J.F., NELSON, S.A., ALLAN, J.F., & CARMICHAEL, I.S.E. 1985. Active rifting in southwestern Mexico: Manifestations of an incipient eastward spreading-ridge jump. *Geology*, **13**(1), 54–57.
- MANEA, M, & MANEA, VC. 2011. Curie point depth estimates and correlation with subduction in Mexico. *Pure and Applied Geophysics*, **168**(8-9), 1489–1499.
- MANN, P. 2007. Global catalogue, classification and tectonic origins of restraining- and releasing bends on active and ancient strike-slip fault systems. *Geological Society, London, Special Publications*, **290**(1), 13–142.
- MARQUEZ, A., OYARZUN, R., & DOBLAS, M. 1999. (ocean-island basalt type) and calc-alkalic volcanism in the Mexican volcanic belt: A case for plume-related magmatism and propagating rifting at an active margin? *Geology*, **22**(1), 51–54.
- PARDO, M., & SUAREZ, G. 1995. Shape of the subducted Rivera and Cocos plates in southern Mexico: Seismic and tectonic implications. *J. geophys. Res*, **100**(B7), 12.357–12.373.
- PEREZ-RAMIREZ, O.G., ESCUDERO-AYALA, C.R., & F.J., NUNEZ-CORNU. 2012. Tomografía telesísmica de la onda-P a nivel de manto superior en el área del bloque de Jalisco, México. *Reunion Anual de la Union Geofisica Mexicana*.
- SBALZARINI, I. F., & KOUMOUTSAKOS, P. 2005. Feature point tracking and trajectory analysis for video imaging in cell biology. *Journal of structural biology*, **151**(2), 182–95.
- SCHELLART, W.P. 2004. Kinematics of subduction and subduction-induced flow in the upper mantle. *J. geophys. Res*, **109**(B07401), 1–19.
- SOTO, L.G., NI, J.F., GRAND, S.P., SANDVOL, E., VALENZUELA, R.W., GUZMÁN-SPEZIALE, M., GÓMEZ-GONZÁLEZ, J.M., & DOMÍNGUEZ-REYES, TONATIUH. 2009. Mantle flow in the Rivera–Cocos subduction zone. *Geophysical Journal International*, **179**(2), 1004–1012.

- STOCK, JM, & LEE, JEFFREY. 1994. Do microplates in subduction zones leave a geological record? *Tectonics*, **13**(6), 1472–1487.
- STUBAILO, I., BEGHEIN, C., & DAVIS, P. M. 2012. Structure and anisotropy of the Mexico subduction zone based on Rayleigh-wave analysis and implications for the geometry of the Trans-Mexican Volcanic Belt. *Journal of Geophysical Research*, **117**(B5), 1–16.
- SUTER, M., LOPEZ-MARTINEZ, M., LEGORRETA-QUINTERO, O., & MARTINEZ-CARILLO, M. 2001. Quaternary intra-arc extension in the central Trans-Mexican volcanic belt. *Geological Society of America Bulletin*, **113**(6), 693–703.
- NIH. 2004. *ImageJ by the National Institutes of Health* <http://rsb.info.nih.gov/ij/index.html>.
- GROUP, MOSAIC . 2009. *Particle tracker by the MOSAIC Group (Models, Simulations, and Algorithms for Interdisciplinary Computing)*, ETH Zurich <http://www.mosaic.ethz.ch/>.
- VERMA, S.P. 2002. Absence of Cocos plate subduction-related basic volcanism in southern Mexico: a unique case on Earth? *Geology*, **30**(12), 1095–1098.
- VERMA, SURENDRA P. 2009. Continental Rift Setting for the Central Part of the Mexican Volcanic Belt: A Statistical Approach. *The Open Geology Journal*, **3**(1), 8–29.
- VIGOUROUX, N., WALLACE, P. J., & KENT, A.J.R. 2008. Volatiles in High-K Magmas from the Western Trans-Mexican Volcanic Belt: Evidence for Fluid Fluxing and Extreme Enrichment of the Mantle Wedge by Subduction Processes. *Journal of Petrology*, **49**(9), 1589–1618.
- YANG, T., GRAND, S.P., WILSON, D., GUZMAN-SPEZIALE, M., GOMEZ-GONZALEZ, J.M., DOMINGUEZ-REYES, T., & NI, J. 2009. Seismic structure beneath the Rivera subduction zone from finite-frequency seismic tomography. *Journal of Geophysical Research*, **114**(B01302), 1–12.